FIELD STUDY OF COMPOSITE PILES IN THE MARINE ENVIRONMENT

Christopher D. P. Baxter, Antonio Marinucci,
Aaron S. Bradshaw and Russell J. Morgan
University of Rhode Island

July 2005

URITC PROJECT NO. 536153

PREPARED FOR

UNIVERSITY OF RHODE ISLAND
TRANSPORTATION CENTER

1. Report No	2. Government Accession No.	3. Recipient's Catalog No.
URITC FY01-03	N/A	N/A

4. Title and Subtitle	5. Report Date
Field Study of Composite Piles in the Marine Environment	July 2005
	6. Performing Organization Code: N/A

7. Authors(s)	8. Performing Organization Report No.
Christopher D. P. Baxter, Antonio Marinucci, Aaron S. Bradshaw, and Russell J. Morgan	N/A

9. Performing Organization Name and Address	10. Work Unit No. (TRAIS)
URI Departments of Ocean/Civil and Environmental Engineering Sheets Building, Narragansett, RI 02882-1197 (401) 874-6575 baxter@oce.uri.edu	N/A
	11. Contract or Grant No.: URI 536153
	13. Type of Report and Period Covered: Final

12. Sponsoring Agency Name and Address	14. Sponsoring Agency Code
University of Rhode Island Transportation Center Carlotti Administration Building, 75 Lower College Road Kingston, RI 02881	

15. Supplementary Notes

N/A

16. Abstract

The regional state-of-the-practice for the construction of pile foundations, fender systems and earth retention systems in the marine environment is to use materials such as timber, steel and concrete. These materials are highly susceptible to attack by marine borers, corrosion, and decay. A possible alternative to traditional piling systems is the use of composite piles constructed of fiber-reinforced polymers (FRP) or high-density polyethylene (HDPE). Composite piles have advantages over traditional piles including complete resistance to marine borer attack and corrosion. The primary objectives of this research were to improve the understanding of the performance of composite piles as a fendering system in the marine environment (1) during installation and (2) during normal fendering conditions. Technical issues studied include the short-term stresses generated during hard driving conditions and short-term behavior and displacement due to lateral impact loading. This was accomplished through two separate field studies in which concrete-filled FRP pipe piles and steel reinforced plastic piles were installed at a residential site in Old Greenwich, CT and along a pier at Fort Wetherill in Jamestown, RI. The piles in Old Greenwich were driven to failure with a hydraulic hammer and PDA and CAPWAP analyses were performed. The piles at Fort Wetherill were impacted with an 85 ton vessel at low speeds and the dynamic response of the piles was measured using accelerometers and displacement transducers. The results of this research provide useful field data for designers and researchers who want to evaluate the effectiveness of composite piles as fender piles.

17. Key Words	18. Distribution Statement
Composite Piles, Impact Loading, Fender Pile, Driving Stresses	No restrictions. This document is available to the Public through the URI Transportation Center, Carlotti Administration Building, 75 Lower College Rd., Kingston, RI 02881

19. Security Classif. (of this report)	20. Security Classif. (of this page)	21. No. of Pages	22. Price
Unclassified	Unclassified	68	N/A

Form DOT F 1700.7 (8-72) Reproduction of completed page authorized (art. 5/94)

Table of Contents

1.0 Introduction....1
2.0 Background on the Types of Composite Piling....2
2.1 Types of Composite Materials....2
2.1.1 Steel pipe core pile....2
2.1.2 Structurally Reinforced Plastic (SRP) Pile....3
2.1.3 Concrete-filled Fiberglass Pipe (FRP) Pile....3
2.1.4 Fiberglass Pultruded Pile....3
2.1.5 Fiber Reinforced Plastic Piling (Plastic Lumber)....3
2.2 Applications....5
2.2.1 Foundation Systems....5
2.2.2 Marine Piling....5
2.3 Advantages and Disadvantages for Marine Applications....5
2.3.1 Interface Bond Effects....6
2.3.2 Drivability....6
3.0 Analysis of Driving Stresses and Pile Integrity During Hard Driving....8
3.1 Background....8
3.2 Site Conditions....8
3.3 Description of Test Piles....10
3.4 Field Testing Methodology....10
3.4.1 Pile Integrity Testing (PIT)....10
3.4.2 Pile Driving Equipment....11
3.4.3 Dynamic Pile Testing....11
3.5 Pile Driving Results....11
3.5.1 Observations during Pile Installation....11
3.5.2 Instrumentation Problems during Installation....13
3.5.3 Pile Integrity....14
3.5.4 Hammer Efficiency....15
3.5.5 Pile Driving Stresses....15
3.5.6 Dynamic Pile Capacities/Parameters....15
4.0 Field Impact Tests of Composite Fender Piles....17
4.1 Background....17
4.2 Site Conditions....18
4.3 Pile Installation....19
4.4 Field Testing Methodology....21
4.4.1 Test Configuration....21
4.4.2 Instrumentation....23
4.5 Data Processing....24
4.6 Dynamic Response of Impact Tests....27
4.6.1 Corrections to Accelerometer Data....29
4.6.2 Impact Energy and Evaluation of Fender Pile Stiffness....30
5.0 A New Dynamic Model for Analysis and Design of Fender Piles....32
5.1 Description of the Dynamic Model....32
5.1.1 Mass Matrix....36
5.1.2 Stiffness Matrix....36

5.1.3 Damping....38
5.2 Comparison of Model and Field Impact Test Results....39
5.2.1 Test Configuration and Results....39
5.2.2 Mass Parameters....40
5.2.3 Stiffness Parameters....40
5.2.4 Damping Parameters....42
5.2.5 Comparison of Field Test and Model Data....42
6.0 Conclusions....45
7.0 Acknowledgements....46
8.0 References....47
Appendix A: MATLAB code....49
Appendix B: Acceleration and Displacement Results....57

List of Tables

Table 2.1. Common types of composite piling (after Iskander and Hassan 1998).....2
Table 2.2. Composite piles used in foundation applications. 5
Table 2.3. Composite piles used in marine applications.....5
Table 3.1. Summary of test pile properties.....10
Table 3.2. CAPWAP results for the PPI pile.....16
Table 4.1. Refusal depths determined by Split-spoon Sample Tests.....18
Table 4.2. Maximum displacements for FRP and PPI pile tests for each accelerometer (see Figure 4.7 for location). 27
Table 4.3. Summary of average vessel and fender pile parameters.....31
Table 5.1. Summary of maximum lateral pile displacements (in cm) recorded during the impact tests. 40
Table 5.2. Summary of velocities measured at the vessel impact point (ACC 2). The damping ratio was calculated from the velocities using Equation (5-18).40

List of Figures

Figure 2.1. Steel core piling manufactured by Plastic Pilings, Inc. 3
Figure 2.2. a.) Steel reinforced plastic pile (Plastic Pilings, Inc.) and b.) Concrete-filled FRP pipe pile (Lancaster Composite). 4
Figure 2.3. Different composite pile types (from Iskander and Stachula 2001)....4
Figure 2.4. Delamination of a concrete-filled FRP pipe pile during a four point bending test (Lampo et al. 1998). 7
Figure 3.1. Site location. 9
Figure 3.2. Profile of Boring No.6 (obtained from Heller & Johnson). 9
Figure 3.3. Michael Sutyla of Heller and Johnsen performing PIT. 10
Figure 3.4. a.) Deformed pile top and b.) exposed steel at the pile tip due to hard driving conditions. 12
Figure 3.5. a.) Setup and installation of FRP pile, and b.) Damage to the pile top after driving. 13
Figure 3.6. PIT plots of the FRP pile (a) before driving and (b) after driving. 14
Figure 3.7. PIT plots of the PPI pile (a) before driving and (b) after driving. 15
Figure 3.8. Pile driving results from the PPI pile. 16
Figure 4.1. Single fender pile system modeled by Maher et al. (1996). 17
Figure 4.2. a.) Location of test site and b.) layout of test piles. 18
Figure 4.3. Sediment sampling at Fort Wetherill using the URI Large-Diameter Gravity Corer. 19
Figure 4.4. Predriving using a Greenheart timber pile 20
Figure 4.5. Use of W8x28 section to prevent bending of FRP pile during handling. 20
Figure 4.6. Damage to the a.) PPI pile and b.) FRP pile during installation. 21
Figure 4.7. Cross-section of test layout, including location of instrumentation. 22
Figure 4.8. Setup for impact load tests. 22
Figure 4.9. a.) Kistler 8305A differential (top) and 8310A single-ended (bottom) accelerometers, and b.) mounting an accelerometer on the pile (Kistler, 2004). 23
Figure 4.10. Massa M-5000 Smart Ultrasonic Sensor (Massa, 1998). 23
Figure 411. Filtered and unfiltered acceleration signals from FRP Pile impact test 4. 25
Figure 4.12. Filtered acceleration and displacement graphs for FRP pile impact Test 4. 26
Figure 4.13. Acceleration, velocity and displacement response for FRP pile impact test 4. 26
Figure 4.14. Acceleration and displacement response of the FRP pile (a and b) and the plastic pile (c and d) during impact. 28
Figure 4.15. Acceleration signal (top) and correction function (bottom). 29
Figure 4.16. Corrected velocity (top) and displacement (bottom) time histories. 30
Figure 5.1. Schematic of the dynamics of a vessel impacting a fender pile: (a) prior to impact, (b) at time of impact, (c) after impact, and (d) after decoupling. 33
Figure 5.2. Schematic of the dynamic fender pile model. 33

Figure 5.3. Typical velocity and displacement time history (Test 3)
as integrated from the accelerometer mounted at the vessel impact point. 39
Figure 5.4. Results of 4-Point bending test performed on a 12.75-inch diameter
Landcaster CP 40 pile (after Rutgers 1996). The tangent modulus
evaluated at 20% of the failure load is shown by the line. 41
Figure 5.5. Results of the static compression test performed on a
section of rubber fender. 42
Figure 5.6. Modeled displacement at the impact point using an
average vessel velocity of 0.12 m/s and 19% damping. 43
Figure 5.7. Comparison of modeled and average measured displacements
along the length of the pile for an average vessel velocity of 0.12 m/s……44

1.0 Introduction

The regional state-of-the-practice for the construction of pile foundations, fender systems and earth retention systems in the marine environment is to use materials such as timber, steel and/or concrete. These materials are highly susceptible to attack by marine borers, corrosion, and decay. The recent environmental improvement of America's harbors has actually accelerated the damage done to timber piles by improving conditions for species of marine borers such as Limnoria and Tordo Novalis. Most timber piles are chemically treated with creosote or copper-chrome-arsenic (CCA) to resist such attack, but these chemicals themselves can pollute the environment and harm marine life (Iskander and Hassan, 1998; Iskander and Stachula, 1999).

A possible alternative to traditional piling systems is the use of composite piles constructed of fiber-reinforced polymers (FRP) or high-density polyethylene (HDPE). Two common configurations for these piles are a FRP pipe pile filled with concrete or a recycled plastic pile reinforced with steel or fiberglass. A recent analytical study on the drivability of composite piles concluded that several technical issues must be overcome before these piles are widely used in practice (Iskander et al. 2001). These issues included the instrumentation, installation, and loading of composite piles under field conditions, analysis of driving stresses, and the durability of composite piles in the field. Presently, there are no well-documented field studies in the literature of the dynamic response of composite fender pile systems.

The primary objectives of this research study were to improve the understanding of the performance of composite piles as a fendering system in the marine environment. Specific areas of study included an evaluation of driving stresses during hard driving conditions (i.e. bedrock) and the response of composite piles to lateral impact loads.

This was accomplished through separate field studies in which concrete-filled FRP pipe piles and steel reinforced composite piles were installed at a residential site in Old Greenwich, CT and along a pier at Fort Wetherill in Jamestown, RI. The piles in Old Greenwich were driven to failure with a hydraulic hammer and PDA and CAPWAP analyses were performed. The piles at Fort Wetherill were impacted with an 85 ton vessel at low speeds and the dynamic response of the piles was measured using accelerometers and displacement transducers. This data was used to develop a dynamic approach to the analysis of fender piles where the impacting vessel coupled with the fender pile is modeled as a freely vibrating, multi-degree of freedom structure with lumped masses, stiffness, and damping. The response of the coupled vessel and fender pile was evaluated using a modal approach along with analytical solutions to the equation of motion. Mass, stiffness, and damping parameters were derived for the fender pile system.

This report is divided into six chapters. Because these piles have not been used extensively in New England for marine applications, chapter two presents a review of the literature on composite piles. This includes the different types of composite piles that are commercially available as well as their potential advantages and disadvantages.

The evaluation of the stresses induced during hard driving conditions is presented in Chapter 3, and Chapter 4 presents the results of the field impact load tests. Chapter 5 presents the new dynamic model for fender pile analysis and design, and a summary of the results are presented in Chapter 6.

2.0 Background on the Types of Composite Piling

There are various manufacturers that produce different types of composite piles currently for the U.S. market. This section presents an overview of the different types of composite piles and possible applications for composite piling. Potential advantages and disadvantages of composite piling in marine applications are also included.

2.1 Types of Composite Materials

Most composite piles are fabricated from either thermoplastic or thermoset polymer resins (Lampo et al, 1998). Thermoplastic materials can be heated and cooled numerous times without undergoing significant chemical compositional changes. Typical thermoplastics include polyethylene (PE), polypropylene (PP) and polyvinyl chloride (PVC). Composite piling manufactured with these materials is called high-density polyethylene (HDPE) piles and typically use, among other components, recycled milk containers as a predominant source of the HDPE. Composite piles are reinforced with fiberglass fibers, steel rebar or steel pipe sections and typically include additives to improve the pile's durability and ultraviolet (UV) resistance (Lampo et. al. 1998; Iskander and Stachula 1999). Conversely, thermoset materials are a one-time reaction material. That is, once the thermoset material chemically reacts and forms bonds, the process is complete and irreversible. Two typical thermoset resins are polyester and vinyl ester. Piling constructed of polymer material have a greater density and weight than timber, and sometimes the polymer is foamed in order to make the pile lighter (Iskander and Hassan 1998).

This section presents the most common types of composite piling that have been used in actual applications as well as in field and laboratory studies. Table 2.1 presents the composite piling to be discussed in subsequent sections.

Table 2.1. Common types of composite piling (after Iskander and Hassan 1998)

Pile Type	Manufacturer	Description
Steel Pipe Core Pile	Plastic Pilings, Inc.	Steel pipe encased by a recycled plastic shell
Structurally Reinforced Plastic Pile	Plastic Pilings, Inc. Seaward International, Inc.	Recycled plastic pile reinforced with fiberglass or steel rebar
Concrete-filled Fiber Reinforced Pipe (FRP) Pile	Lancaster Composite, Inc. Hardcore Composite, Inc.	Fiberglass tubular section filled with concrete
Fiberglass Pultruded Pile	Creative Pultrusion	Fiberglass cross-section filled with a fiberglass grid inserts
Fiber Reinforced Plastic Pile	U.S. Plastics	Recycled plastic pile with fiberglass reinforcement

2.1.1 Steel pipe core pile

Steel pipe core piles were the first composite piles introduced to the U.S. market (Iskander and Stachula 1999). This type of pile is comprised of a steel pipe core, the structural component, which is encased by a 4 to 8 inch plastic shell, which provides corrosion and degradation protection. The composite piles are typically 8 to 24 inches in outside diameter, and have been manufactured as long as 75 feet. A representative cross section is shown in Figure 2.1. Early versions of this pile delaminated at the interface between the plastic shell and the steel core (Iskander and Stachula 1999).

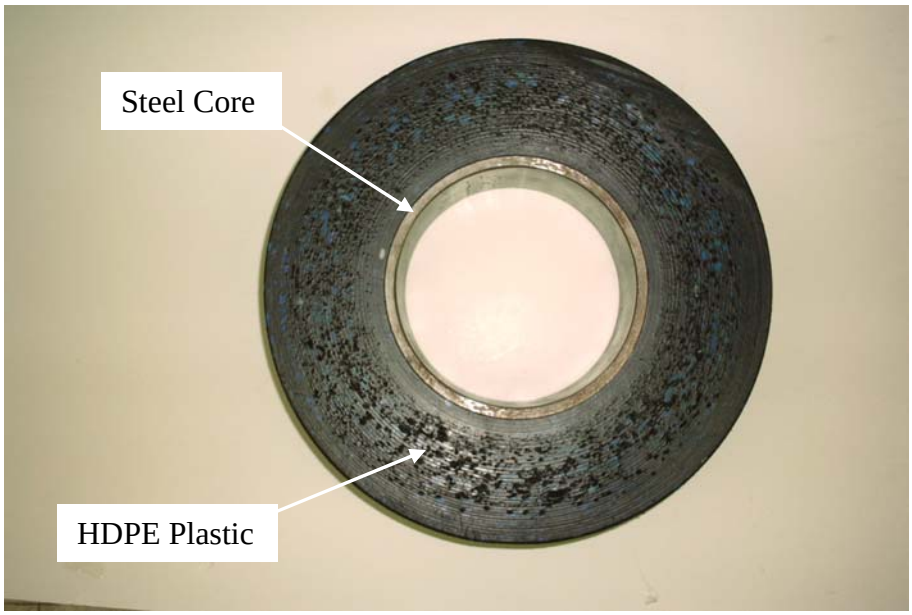

Figure 2.1. Steel core piling manufactured by Plastic Pilings, Inc.

2.1.2 Structurally Reinforced Plastic (SRP) Pile

Structurally reinforced plastic (SRP) piles consist of HDPE plastic reinforced with either fiberglass rods or steel rebar (Iskander and Stachula 1999), as shown in Figure 2.2a. The outer surface of SRP piles is typically treated to retard UV degradation. SRP piles are available in diameters between 10 and 17 inches and are reinforced with 6 to 16 rods or rebar, with diameters ranging from 1 to 1.4 inches. These piles can be produced in a variety of lengths.

2.1.3 Concrete-filled Fiberglass Pipe (FRP) Pile

Concrete-filled fiberglass pipe (FRP) piles, as the designation implies, are pipe piles comprised of a fiberglass shell and concrete infill, as shown in Figure 2.2b. The fiberglass shell provides the pile's tensile strength while the concrete infill provides flexural rigidity and resistance to buckling. The outer coating retards UV degradation and protects against chemical damage and abrasion. Hardcore piles are filled with concrete after installation, whereas Lancaster Composite piles are filled with concrete prior to installation. These piles are available in a variety of lengths with outside diameters ranging from 8 to 18 inches.

2.1.4 Fiberglass Pultruded Pile

Fiberglass pultruded piles are comprised of a fiberglass pipe pile, fitted with fiberglass grid inserts. Figure 2.3 presents a typical cross section for the pultruded pile along with other composite pile types. In fendering applications, the HDPE shell and fiberglass inserts are used, among other things, to absorb vessel impact (Iskander and Stachula 1999).

2.1.5 Fiber Reinforced Plastic Piling (Plastic Lumber)

"Plastic Lumber" is comprised of recycled plastic and fiberglass reinforcement (Iskander and Stachula 1999). The outer portion of the pile's cross-section is dense and solid, whereas the inner portion of the cross-section is foam-filled to reduce the pile's weight. These piles are typically 10 inches in diameter and 25 feet in length.

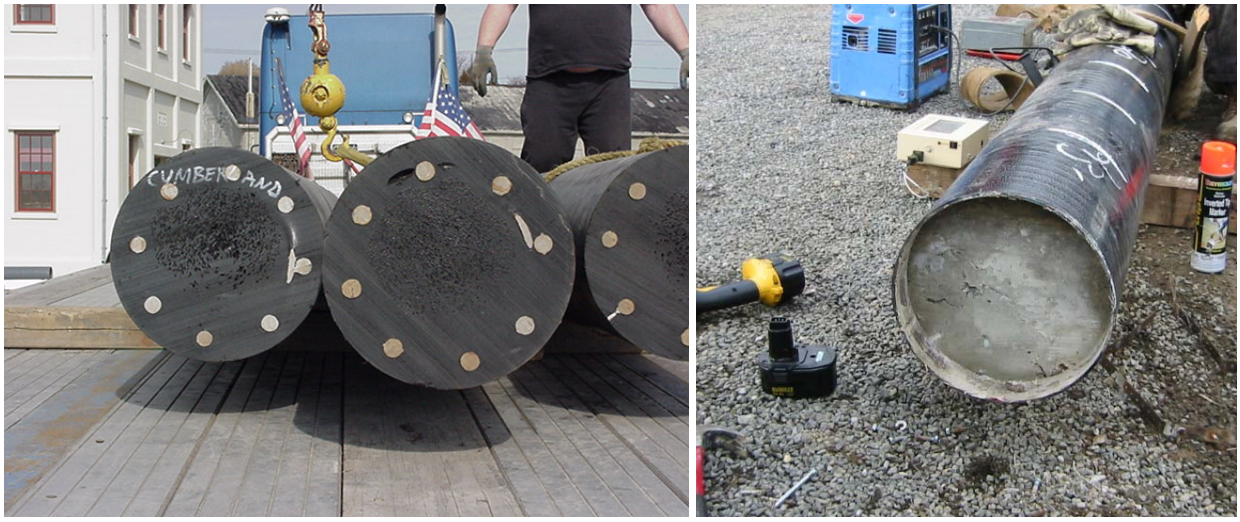

(a) (b)

Figure 2.2. a.) Steel reinforced plastic pile (Plastic Pilings, Inc.) and b.) Concrete-filled FRP pipe pile (Lancaster Composite).

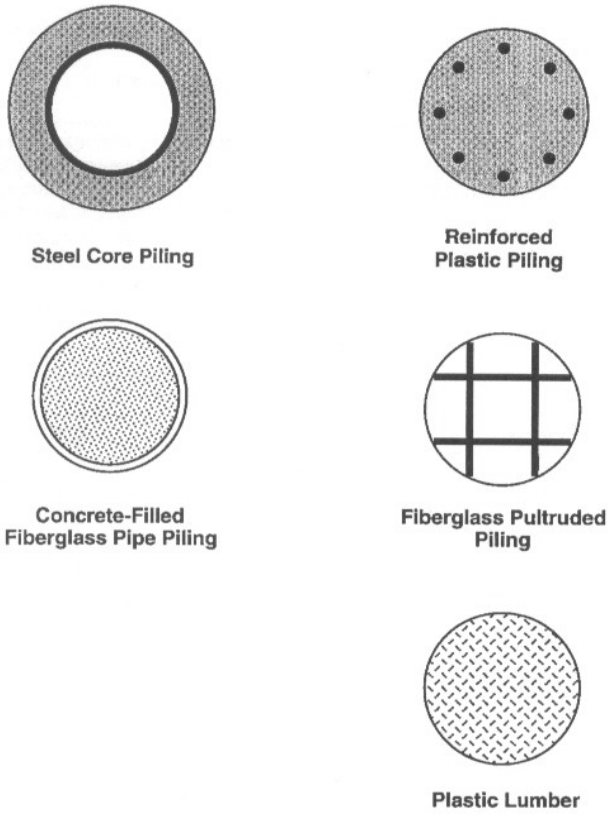

Figure 2.3. Different composite pile types (from Iskander and Stachula 2001).

2.2 Applications

2.2.1 Foundation Systems

According to published literature, composite piling has been rarely used in structural foundation applications. Table 2.2 provides a select listing in which composite piles have been installed and tested under typical foundation conditions.

Table 2.2. Composite piles used in foundation applications.

Composite Pile Type	Application	Location	Reference
Concrete-filled FRP Pile	Studied Driving Stresses and Bearing Capacity	Asbury Park, New Jersey	Goble et al. 2000
Hardcore Fiberglass shell; concrete infill	Dynamic Analysis and Driving Cond. Study	New Castle, Delaware	Kozera 1997
Concrete-filled FRP Pile	Dynamic Analysis and Driving Cond. Study	Rte 351; Chesapeake Bay area, Virginia	Pando et al. 2003
Structurally Reinforced Plastic (SRP) Piles	Dynamic Analysis and Driving Cond. Study	Rte 351; Chesapeake Bay area, Virginia	Pando et al. 2003
Concrete-filled FRP Pile	Bridge Bent Foundation Support	Rte 40; Nottoway River, Virginia	Pando et al. 2004

2.2.2 Marine Piling

Unlike the limited use in structural foundation systems, composite piling has been used increasingly in marine applications, most notably in fender systems/piling. Table 2.3 provides a select listing in which composite piles have been installed in marine applications.

Table 2.3. Composite piles used in marine applications.

Composite Pile Type	Application	Location	Reference
Steel Pipe Core Piling	Anchor Floating Docks	Ferry Docks, Newport, RI	N/A
Fiberglass Pultruded Pile	Fender Piling	Tiffany Street Pier in NY, NY	Lampo et al. 1998
Structurally Reinforced Plastic (SRP) Piles	Fender Piling	Port Newark in Newark, NJ	Lampo et al. 1998
Fiberglass Pultruded Pile	Fender Piling	Port Newark in Newark	Lampo et al. 1998
Fiber Reinforced Plastic Piling (Plastic Lumber)	Fender Piling	Port Newark in Newark	Lampo et al. 1998

2.3 Advantages and Disadvantages for Marine Applications

As compared to traditional piling materials, composite piles present numerous potential advantages, including the following (from Iskander and Stachula 1999, 2001; Lampo et al. 1998):

- Composite piles use plastics, which would otherwise be disposed in landfills.
- Composite piles are resistant to marine borers.
- Composite piles do not leach hazardous chemicals into the environment.
- Composite piles may have much lower life-cycle costs than traditional piles.
- Disposal is not problematic since composites are not manufactured or treated with hazardous materials.

- When used in fendering applications, some composite pile types have been reported to absorb as much as 40 times more energy than traditional timber piles.

Conversely, composite piles also have inherent disadvantages, including the following (from Iskander and Stachula 1999, 2001; Iskander and Hassan 1998; Lampo et al. 1998):

- The initial cost of composite piles is two to three times more expensive.
- Due to their low stiffness, composite pile installation is typically less efficient and more difficult than traditional piling, as explained in a subsequent section.
- Composite piles having low stiffness can cause handling and installation problems.
- Interface bonding and delamination is an ongoing concern, as explained in a subsequent section.

Another potential disadvantage is illustrated by the Tiffany State Pier case study referenced in Table 2.3. In 1996, the pier was destroyed by a major fire. The high density polyethylene piles were severely damaged by the fire, and the pier was closed the following year. This illustrates the need for adequate fire protection of composite pile materials.

2.3.1 Interface Bond Effects

As reported in numerous published works, ineffective interface bonding between the different materials (e.g. steel and plastic, FRP and concrete) in composite piles was a significant problem in early designs (e.g. Iskander and Stachula 1999; Iskander and Hassan 1998). Figure 2.4 provides an example of interface delamination between the concrete core and the FRP shell during a flexure test. The concrete-filled fiberglass pipe pile was tested in four point bending and, during the test, the squeezing out of concrete occurred. This delamination clearly indicates debonding at the interface between the FRP shell and the concrete core. In the recent past, it has been reported by various authors referenced throughout this text that manufacturers have altered the fabrication process to minimize the occurrence of delamination. For example, in some instances, the inside surface of the FRP shell is roughened to improve the mechanical interface bond. In addition, bonding agents have been used on the inside surface of the shell prior to infilling with concrete. Expansive concrete has also been used in the core (Rizkalla and Fam 1999).

In concrete–filled FRP piles, the concrete core must be well connected to the shell material. This is accomplished by using a non-smooth FRP interface surface or by using bonding agents. If there is insufficient interface bond between the shell and the core, the concrete fill will delaminate from the composite shell, thereby resulting in independent material behavior rather than composite.

2.3.2 Drivability

Composite materials, in general, have been reported to have a higher damping coefficient and lower stiffness than traditional materials. Highly damped, low stiffness piles are more difficult to drive due to the difficulty in transferring driving energy to the pile. Iskander and Hassan (1998) reported that the modulus of elasticity, (typically not provided by the manufacturer) and the pile's specific weight has a profound influence on the drivability of HDPE reinforced piles. Conversely, concrete-filled FRP pipe piles have been reported to have a higher stiffness and a low damping coefficient due to its concrete core. According to Iskander and Hassan (1998), FRP piles are easier to drive and have an overall driving behavior similar to purely concrete piles

(Iskander and Hassan 1998). However, there is limited published information pertaining to composite pile drivability.

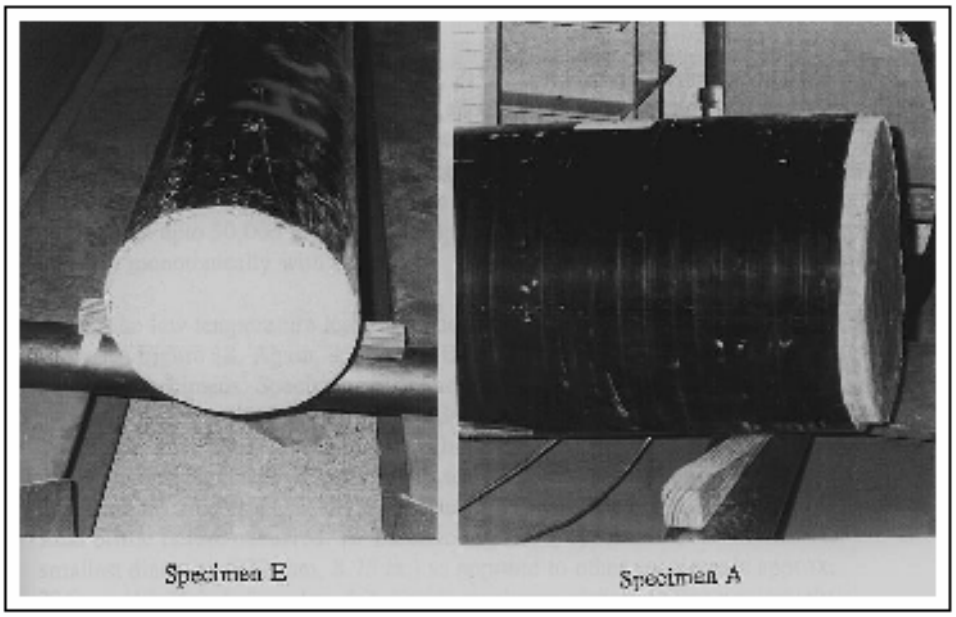

Figure 2.4. Delamination of a concrete-filled FRP pipe pile during a four point bending test (Lampo et al. 1998).

3.0 Analysis of Driving Stresses and Pile Integrity During Hard Driving

3.1 Background

Numerous studies have been performed on the drivability of composite piles. However, many of these studies are theoretical in nature and do not evaluate actual pile driving in the field. For example, Iskander et al. (2001) and Iskander and Stachula (2002) used a wave equation model (WEAP) to study the influence of the modulus of elasticity, damping, and unit weight on the drivability of three types of composite piles. These studies report that driving resistance (hammer blows) decreases appreciably with either a decrease in (1) the pile's elastic modulus or (2) the pile's unit weight, especially below a unit weight of about 110 pcf. Conversely, damping was shown to have a negligible effect on drivability.

Iskander et al. (2001) used WEAP to compare the drivability of short (60 ft), low capacity piles and long (90 ft), high capacity composite piles in a typical marine soil profile. The results indicate that the drivability of reinforced plastic (plastic lumber) piles, concrete-filled fiberglass pipe (FRP) piles, and timber piles was not a problem for the short, low capacity piles. However, the drivability (i.e. ease of installation) of these pile types is very different for the long, high capacity piles.

Iskander and Stachula (2002) back evaluated WEAP parameters (modulus of elasticity, damping and unit weight) by matching the results to PDA results obtained during driving of the plastic lumber and the FRP piles. Based on this analysis the authors recommend the following parameters for the plastic lumber piles: an elastic modulus equal to 2/3 of the manufacturer's reported composite modulus, the manufacturer's reported unit weight, and a pile damping factor of 9. Typical WEAP parameters published for traditional prestressed concrete piling provided a good match to measured results for the FRP pile.

Wave equation analyses such as PDA, CAPWAP and WEAP have been used in practice for the design of composite piles (Kesavanathan and Kozera, 1997; Goble 2000). However, there is limited data supporting the reliability of these methods to model the non-linear behavior of composite piles. Clearly, there is a need for continued study of pile driving in the field.

This chapter presents the results of pile driving on two types of composite piles in Old Greenwich, Connecticut. The piles were driven to failure to measure the driving stresses and evaluate methods for detecting damage. An expanded treatment of this portion of the study can be found in Gummert (2003).

3.2 Site Conditions

The composite piles used in this study were installed using an impact hammer at an existing residential construction site in Old Greenwich, Connecticut, shown in Figure 3.1. Due to the proximity to the waterfront, the high groundwater table and soft soils, timber piles were installed to support the structure. Since the pile driving equipment was already on site, the project provided a unique opportunity to drive composite piling for this study.

The subsurface conditions were evaluated from 6 borings previously performed at the site by Heller and Johnsen. A typical boring log (No. HJ-6) from the site is shown in Figure 3.2. The subsurface conditions consist of alternating layers of silt and sand overlying bedrock. Bedrock was encountered at various depths across the site ranging from 13.5 to 16.5 feet, and the

upper 1.5 feet of the bedrock was in a weathered condition. The composite test piles used in this study were installed adjacent to Boring No. HJ-6.

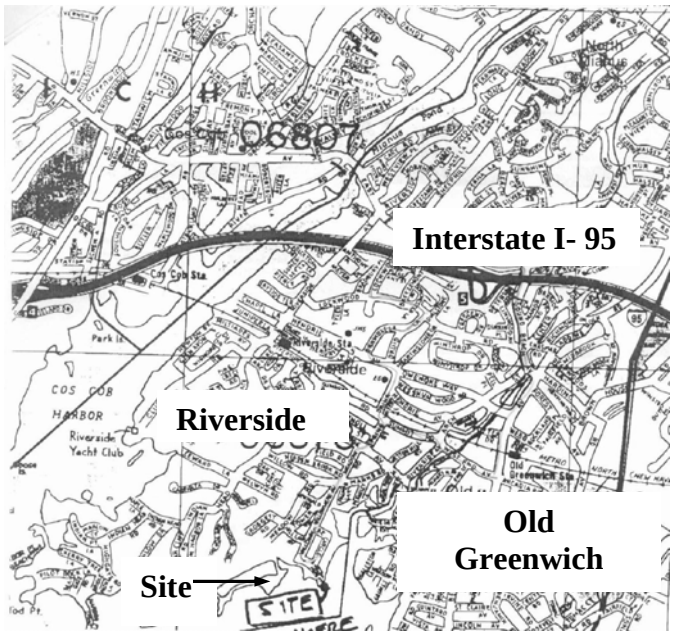

Figure 3.1. Site location.

HELLER AND JOHNSEN
FOOT OF BROAD STREET
STRATFORD, CONNECTICUT

PROJECT: 51 Willowmere Circle
LOCATION: Old Greenwich, CT
FILE NO.: 58201

BORING NO.: HJ-6
SHEET NO.: 1 OF 1
DATES: 08/29/02-08/29/02

CONTRACTOR: Hardiman Company & Associates, Inc.
FOREMAN: Tony Scaife
ENGINEER: Brian D. Opp

GROUNDWATER READINGS (4)

DATE	TIME	DEPTH
8/29/02	1400	4.25'
8/30/02	0900	5.9'

	CASING	SAMPLER	CORE BARREL
TYPE	HSA	SS	
SIZE I.D.	2 3/4"	1 3/8"	
HAMMER WT.		140 lbs.	BIT
HAMMER FALL		30 in.	

G.S. ELEV. 7.8 ft.
DATUM NGVD 1929
LOCATION See Plan
TIME AT COMP. 1200

DEPTH	CASING BLOWS	SAMPLE NO.	TYPE	PEN./REC.	DEPTH	BLOWS/6" (CORING TIME)	SAMPLE DESCRIPTION	REMARKS	STRATUM DESCRIPTION
		S-1	SS	24/9	0-2.0	3-3-3-3	Top 2": TOPSOIL, (Grass, Roots, Loam) Bottom 7": Light brown, dark brown, fine to medium SAND, some Silt, some Cobble, trace Root.		TOPSOIL 0.2' SILTY SAND (FILL)
5		S-2	SS	24/0	5.0-7.0	1-2-2-9	Loose, grey, fine to coarse SAND and Gravel, some Silt.		4.0' ORGANIC SILT 6.5' GREY, SILTY SAND
10		S-3	SS	24/7	10.0-12.0	18-30-34-50	Top 3": Grey, blue SILT, little fine to medium SAND. Bottom 4": Brown, fine to medium SAND, some Silt.	1	10.3' BROWN SILTY SAND
15		S-4	SS	0/0	15.0	100		2 3	13.5' WEATHERED ROCK 15.0' E.O.B.
20									

Figure 3.2. Profile of Boring No.6 (obtained from Heller & Johnson).

3.3 Description of Test Piles

Two types of composite piles were tested: a steel reinforced plastic pile (PPI) and a concrete-filled fiberglass pipe (FRP) pile. The solid plastic pile, manufactured by Plastic Pilings, Inc., was fabricated from recycled plastic and was reinforced with eight, 1-inch diameter steel rebar. The FRP pile, manufactured by Lancaster Composite, had a shell thickness of 0.8 inches. Table 3.1 presents the respective pile properties.

Table 3.1. Summary of test pile properties.

Pile Type	Length (ft)	Diameter (in)	Unit Weight (lb/ft^3)	Modulus of Elasticity[1] (lb/ft^2)
PPI	24	13.25	68	1,586
FRP	24	10	145	4,500

Notes:
1. Values reported by Manufacturer.

3.4 Field Testing Methodology

3.4.1 Pile Integrity Testing (PIT)

Pile Integrity Testing (PIT), as shown in Figure 3.3, was performed before and after pile installation to evaluate pile damage, if any, caused by pile driving. The testing was performed in accordance with ASTM D5882, "Standard Method for Low Strain Integrity Testing of Piles". The PIT is performed by striking one end of the pile with a small, instrumented hammer and then measuring the stress wave with an accelerometer attached to the same end of the pile. Reflections of the stress wave occur at changes in pile impedance (i.e. at boundaries, density changes, cross-sectional area changes, etc). For this reason, PIT can be used to detect defects in piles. PIT is most commonly used on concrete piles, however, it was uncertain whether or not PIT could effectively be used on the composite piles.

Figure 3.3. Michael Sutyla of Heller and Johnsen performing PIT.

3.4.2 Pile Driving Equipment

The contractor, Norwalk Marine Contractors, used a Junttan Hydraulic Hammer HHK6 to drive the test piles. The hammer has a rated energy of 5.3 kip-ft (GRLWEAP 2002), a maximum stroke of 4.0 ft, and a helmet weight of 1.323 kips. An aluminum-micarta hammer cushion was used during the installation. The hydraulic hammer was selected because it allowed precise control over the delivered hammer energy. Additionally, hydraulic hammers have a very high efficiency (up to 80%). The hammer energy was increased incrementally during driving from 2.0 kip-ft at the start of driving to 5.3 kip-ft at the end of driving to be able to measure the stresses in the pile up to and at failure.

3.4.3 Dynamic Pile Testing

The Pile Driving Analyzer (PDA) was used to estimate static pile capacity, driving stresses and hammer efficiency during driving. Strain gages and accelerometers are mounted in close proximity to the pile head, and are used to measure force and acceleration signals, with respect to time, for each hammer blow. The PDA uses these signals along with a wave equation model (i.e. Case method) to obtain real-time estimates of static pile capacity, driving stresses, and hammer efficiency. The Case Pile Wave Analysis Program (CAPWAP) is a more rigorous wave equation based model. CAPWAP is a curve fitting routine whereby soil model parameters (i.e. quake and damping) are modified until the modeled force and acceleration signals match the measured signals. A complete discussion of wave propagation theory, PDA and CAPWAP is presented in the Federal Highway Departments manual on driven piles (FHWA 1998).

3.5 Pile Driving Results

3.5.1 Observations during Pile Installation

After instrumenting the PPI pile, installation commenced with the initial driving energy equal to 20,000 ft-lb, which is equivalent to a 1.5 ft hammer stroke. As expected, the driving through the first few feet, approximately 5 blows/ft through silty sand and organic silt, went smoothly. At an approximate depth of 6 ft, the blow counts significantly increased to 108 blows/ft, and the pile barely moved. Shortly thereafter, the pile top began to slightly deform or buckle, which can be attributed to, among other reasons, the energy imparted to the pile by the hammer or by the generation of heat from the driving equipment itself. Driving was eventually stopped at an approximate depth of 6.6 ft when the resistance reached 672 blows/ft. Since the pile did not achieve the expected embedment depth, the pile was believed to have encountered a boulder. The pile was extracted and visually checked for damage. Upon visual inspection, the pile tip clearly deformed and the steel rebar was noticeably exposed.

After inspection, the pile was moved and redriven approximately 3 ft away from the original location using the same energy rating. Driving resistance increased as the installation progressed. At an approximate depth of 7 ft, the driving energy was increased to 31,000 ft-lb. However, due to the large deformation of the pile top, as shown in Figure 3.4a, driving was eventually stopped at an embedment depth of approximately 8.33 ft. The recorded blow count at this depth was 44 blows/ft. Although the test borings indicate that refusal was located at an approximate depth of 15 ft, the pile clearly encountered a boulder or some other obstruction. The PPI pile was then extracted and visually inspected. In addition, PIT was performed on this pile after driving to assess damage, as explained in a subsequent section.

Upon inspection of the pile, the following was noted:

- The top 3 ft of the pile bent out of vertical alignment by slightly more than 3 degrees.
- The diameter at the top of the pile was 14.5 inches instead of 13.25 inches.
- At the pile tip, the plastic surrounding the reinforcement was deformed or missing.
- At the pile tip, the steel rebar was exposed between 0.2 to 0.8 inches, as shown in Figure 3.4b.

(a)

(b)

Figure 3.4. a.) Deformed pile top and b.) exposed steel at the pile tip due to hard driving conditions.

The concrete-filled fiberglass pipe (FRP) pile was then instrumented and installed. However, there were problems attaching the PDA accelerometers and strain gages, as will be discussed in section 3.4.2. Prior to driving, PIT was performed to verify the integrity of the concrete core. A four-inch thick plywood cushion was used to prevent the ram from damaging the top of the pile. In order to avoid the same problems encountered when driving the PPI pile, the FRP was installed away from the PPI pile location.

The first 7 ft of the FRP pile pushed into the soil under the combined self-weight and driving equipment weight. At an embedment of approximately 8 ft, the driving commenced us-

ing a rated energy of 20,000 ft-lb. By a depth of approximately 9 ft, the blow counts exceeded 20 blows/ft. Figure 3.5a shows the installation setup for the FRP pile. Soon after driving commenced, problems with the PDA instrumentation were realized; however, this is explained in greater detail in a subsequent section. Due to the instrumentation problems and the ineffectiveness of the PDA, the pile was extracted to determine whether the pile tip was damaged. After inspecting the pile and finding no appreciable damage, the pile was reattached and redriven. At approximately 12 ft, the energy of the hammer was increased to 52,000 ft-lb. Due to this high energy, the pile cushion broke and the concrete core at the pile top began to crack and spall. At approximately 12.75 ft of embedment, with blow counts equal to 48 blows/ft, driving was stopped in order to extract and inspect the pile for damage. Unfortunately, extraction efforts were unsuccessful. Upon inspection, the pile top was visibly broken, as shown in Figure 3.5b. Since the pile tip could not be inspected, the FRP pile was cut approximately 11.4 ft from the top and PIT was performed on the embedded 12.35 ft portion of the pile to assess pile damage. However, when the FRP pile was extracted after the initial driving in order to reattach the PDA gages, the pile tip did not show appreciable damage.

(a) (b)

Figure 3.5. a.) Setup and installation of FRP pile, and b.) Damage to the pile top after driving.

3.5.2 Instrumentation Problems during Installation

As a requisite part of the Pile Driving Analyzer (PDA) setup, the composite piles were instrumented with two acceleration transducers and two strain gages. GZA Geoenvironmental, Inc. in Norwood, Massachusetts, installed the devices and performed the dynamic testing. The acceleration transducers and strain gages used in conjunction with the PDA were attached approximately 5.0 feet below the top of each composite pile.

Problems with the instrumentation were realized during the installation of the devices and during the installation of the FRP pile itself. The first concern pertained to the location of the devices. In order to obtain accurate dynamic measurements, the instrumentation needs to be in-

stalled as close to the top of the pile as practical. Therefore, the instrumentation was installed approximately 5.0 feet below the top of the pile. However, at this position, the instrumentation was located approximately 4 inches below the FRP shell top. Unfortunately, the instrumentation was attached at the end of adhesive/binding material that is used to create the bond between the FRP shell and the concrete core. During pile installation, the instrumentation became detached, and, as a result, the PDA did not record any measurements. The instrumentation was attached at a new location on the same pile. However, shortly after commencement of pile driving, the instrumentation once again became detached and no measurements were obtained. After analyzing the problem with the instrumentation attachment to the composite pile, it was assumed that the anchors attaching the devices could not expand properly within the concrete core, and therefore kept detaching. No PDA measurements were obtained for the FRP pile.

3.5.3 Pile Integrity

The results from the PIT performed on the FRP pile is shown in Figure 3.6 for conditions (a) before driving and (b) after driving. The signals obtained through the FRP pile were relatively easy to obtain. The wave trace before driving shows a distinct return signal from the pile toe as expected, along with a reflection approximately halfway down the pile. It is anticipated that the latter reflection was attributed to a crack that may have been made during transport or handling of the pile. The calculated wave speed of 14,000 ft/sec is slightly higher than published values of approximately 10,000 ft/sec for concrete (Kindsler et al. 1982). The PIT results obtained after driving shows a highly irregular wave trace suggesting significant cracking and damage to the pile from driving. This is consistent with the very hard driving that the piles were subjected to at the end of installation, as explained in a previous section.

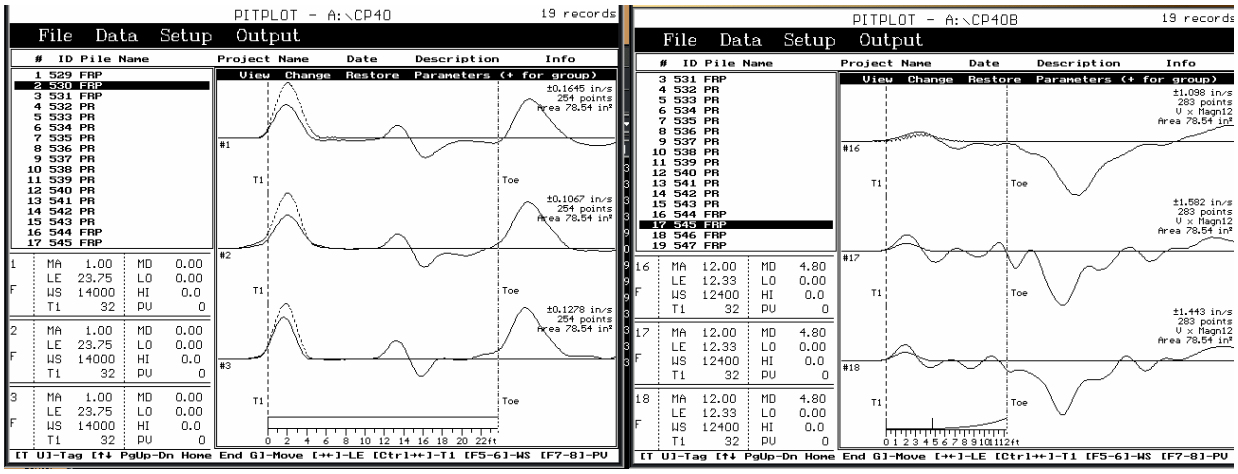

(a) (b)

Figure 3.6. PIT plots of the FRP pile (a) before driving and (b) after driving.

Unlike the FRP pile, signals from the PPI pile were difficult to obtain. The best traces for the PPI pile are shown in Figure 3.7 for conditions (a) before driving and (b) after driving. Both traces show a large reflection at the pile toe and at about 5 ft and 6 ft below the pile top. It is difficult to ascertain if the latter reflection is attributed to air bubbles that are typically found within the plastic matrix or to a defect of concern. The calculated wave speed of 10,500 ft/sec is similar to the published values for concrete. The PIT traces obtained before and after pile driving are very similar, suggesting that driving did not cause fracturing or delamination of the pile.

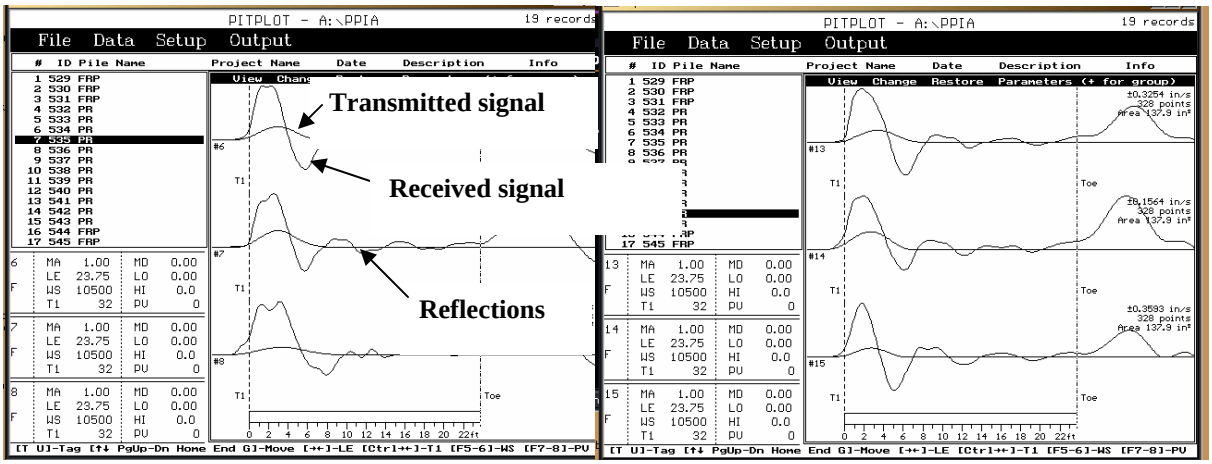

Figure 3.7. PIT plots of the PPI pile (a) before driving and (b) after driving.

3.5.4 Hammer Efficiency

Hammer efficiency is a measure of the percentage of the rated hammer energy that is transferred into the pile. The energy transfer characteristics are therefore related to the type of hammer and type of pile. Typical efficiency values range from 25% for a diesel hammer on concrete/timber piles to 50% for a single-acting air/steam hammer on steel piles (FHWA 1998). The efficiency of the hydraulic hammer, Junttan HHK6, on the PPI pile was estimated. No pile cushion was used during driving. Throughout driving the hammer maintained a stroke of 1.5 feet. The rated energy of 19.85 kip-ft was calculated from product of the hammer weight (13.23 kips) and measured stroke (1.5 ft). The average transferred energy, measured with the PDA over a depth of 4 to 6 feet, was 10.28 kip-ft yielding an average efficiency of 52%, standard deviation of 10%.

3.5.5 Pile Driving Stresses

The manufacturer's published yield stresses for the PPI pile are 3.13 ksi. The maximum compressive stress recorded with the PDA at the pile head, at the end of driving, was 2.28 ksi. Though the driving stresses did not appear to exceed the yield stress, buckling of the pile was observed near the pile head. A photograph of the buckled pile head is shown in Figure 3.4a. The inconsistencies with the measured and observed behavior may be attributed to (1) the proximity of the strain gages to where the yielding took place, (2) uncertainties in the yield stress, or (3) melting of the pile from the heat of the hammer.

3.5.6 Dynamic Pile Capacities/Parameters

A bearing graph is a useful tool in the field for obtaining the hammer blows required to obtain a given pile capacity. A similar relationship was made for the PPI piles by comparing the observed blow counts and the capacities obtained from the PDA. Because the observed blow counts were not taken at exactly the same depth intervals, the observed blow counts and PDA capacities were plotted on separate graphs, as shown in Figure 3.8.

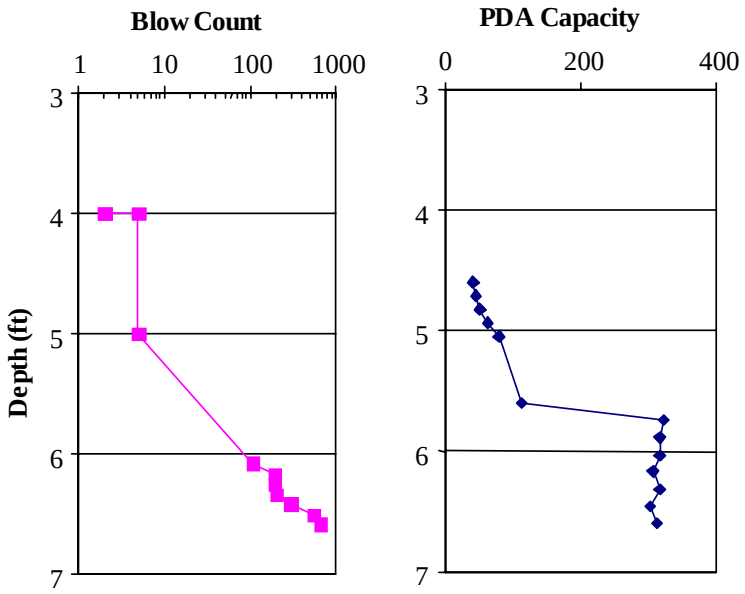

Figure 3.8. Pile driving results from the PPI pile.

As shown in Figure 3.8, the blow counts and capacity increase with depth. The capacity essentially remains constant (approximately 310 kips) below a depth of about 6 ft, while the blow counts increase from 100 to 672 blows/ft. This behavior is counterintuitive since a higher blow count would typically imply a higher capacity. The data show that the PDA capacities therefore may be uncertain for blow counts greater than about 20 to 30 blows per foot. Dynamic capacities can be underestimated for blow counts higher than 10 blows/ft because the full soil resistance cannot be mobilized (FHWA 1998; Fellenius et al. 1989; Rausche et al. 1985).

The results obtained from the CAPWAP analysis performed on the PPI pile at the end of driving are summarized in Table 3.2. The capacity of the pile was predominately in end bearing, which is expected considering that the pile was driven into rock. The total CAPWAP capacity of 303 kips agreed well with the value of 313 kips obtained with the PDA at the same blow number. However, the CAPWAP toe quake parameter obtained in the analysis was much higher than the value of around 0.1 inches typically used in dynamic pile driving analyses. The high toe quake may have contributed to the damage that occurred at the pile tip during hard driving, as shown in Figure 3.4b.

Table 3.2. CAPWAP results for the PPI pile.

Capacity			Quake		Damping	
Shaft (kips)	Toe (kips)	Total (kips)	Shaft (in)	Toe (in)	Shaft (kip-sec/ft)	Toe (kip-sec/ft)
3	300	303	0.1	0.56	0.09	0.008

4.0 Field Impact Tests of Composite Fender Piles

The primary objective of this portion of the study was to observe and understand the dynamic response of composite fender piles under lateral impact loading from a berthing ship. A FRP pile and a PPI pile were impacted under working loads by an 85 ton vessel. Each pile was instrumented with four accelerometers and one displacement transducer to measure its response to the impact. There are currently no measurements of this kind in the literature. This data could be used to study the energy absorbing capabilities of composite fender piles, calibrate numerical models (e.g. Maher et al. 1996), and establish better design procedures for these materials (Military handbook MIL-HDBK-1025/1).

4.1 Background

Although there are no published field studies of impact loading of composite fender piles, numerical analyses have been performed by Maher et al. (1996) at Rutgers University. The objective of the study was to accurately model the soil-pile interaction and load-deformation behavior of fender piles. Both linear and non-linear soil behavior was modeled using the finite element program ABAQUS. Figure 4.1 shows the fender pile configuration that was modeled. The pile was first designed assuming the simple span supports shown in the figure, according to the standard military handbook procedure. For the finite element analyses, the lower support was removed and resistance was provided through soil-pile interaction. The material properties of a Seaward fiberglass reinforced plastic pile were used, with an average modulus of elasticity of 460 ksi (3,169 MPa) and an axial compression strength of 4 ksi (28.25 MPa).

The results indicated that shear and flexural stresses developed in the pile below the embedment point, and the magnitude of stresses on the pile are less than those predicted by the military handbook method. Despite this, plastic soil strain near the pile indictment was observed; even at a small birthing load of 4 kips.

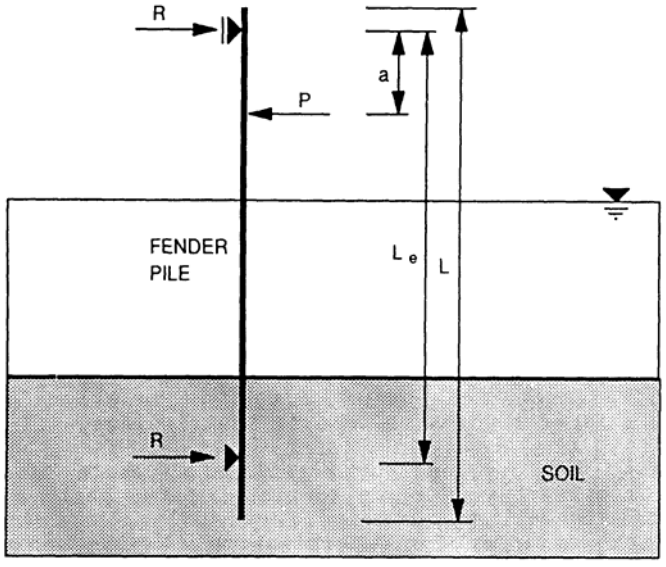

Figure 4.1. Single fender pile system modeled by Maher et al. (1996).

4.2 Site Conditions

The field impact tests were conducted at Fort Wetherill in Jamestown, Rhode Island, as shown in Figure 4.2a. The site is situated along a rehabilitated pier that is part of the Rhode Island Department of Environmental Management Fisheries facility.

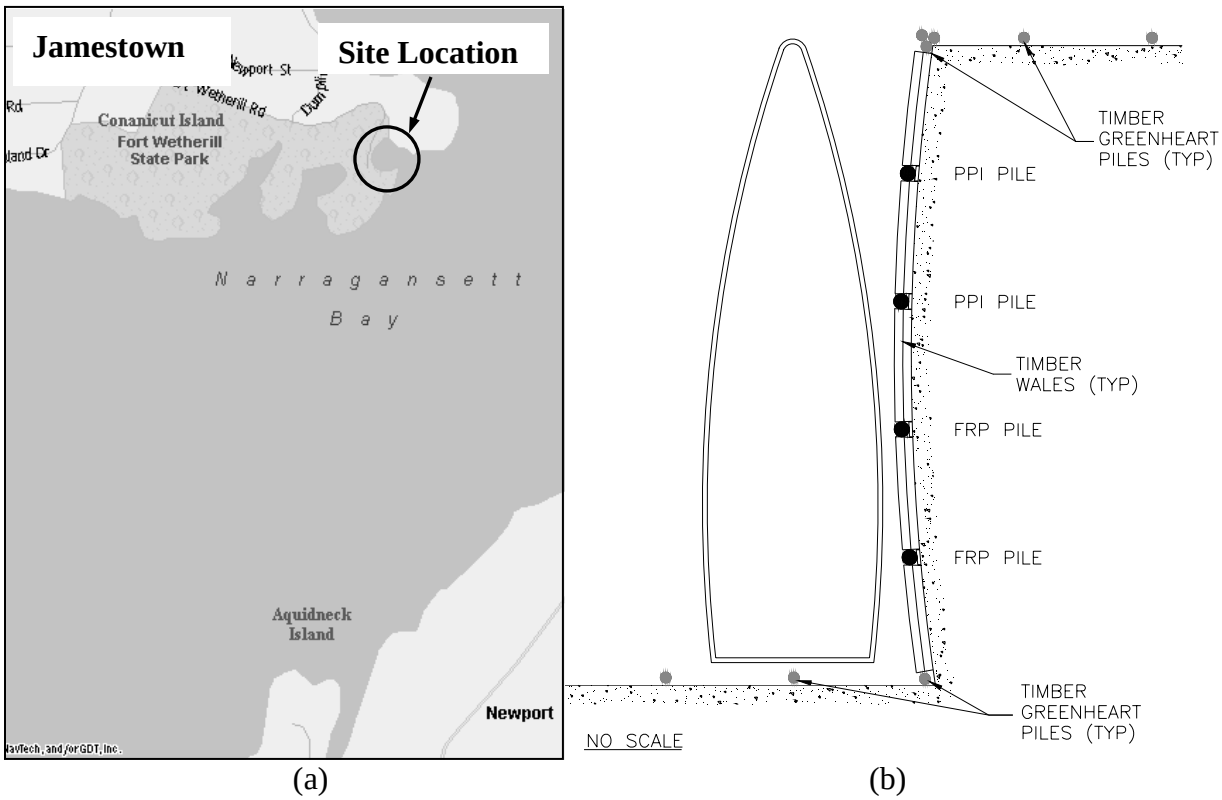

(a) (b)

Figure 4.2. a.) Location of test site and b.) layout of test piles.

A site investigation was performed in the small inlet adjacent to the pier to determine the depth of rock and to the types of soils present at the site. Two large-diameter gravity (LGC) cores and three split-spoon samples (SS) were obtained. The depth of refusal/bedrock was estimated from the sampling and testing, as shown in Table 4.1. The URI LGC consists of a sampling tube with a driving weight and stabilizing fins at the top, as shown in Figure 4.3. This assembly is lowered on a cable until it is approximately 10 ft (3m) above the sediment surface. Once in position, the LGC free falls into the sediment. Once the sample is obtained, a check valve at the top of the apparatus and a special core catcher in the bottom of the sampler hold the sediment in the tube. The LGC apparatus can obtain 4-inch (10.2cm) diameter samples in a PVC or steel core barrel up to 10ft (3m) in length. The URI research vessel, CT-1, was used to perform both the LGC and SS tests in the marina sediments.

Table 4.1. Refusal depths determined by Split-spoon Sample Tests

Location	Water Depth	Refusal Depth
Inner Bay	9.6ft (2.92m)	9.1ft (2.78m)
Corner of Pier	6.3ft (1.91m)	7.9ft (2.41m)
Outer Bay	12ft (3.67m)	11.4ft (3.48m)

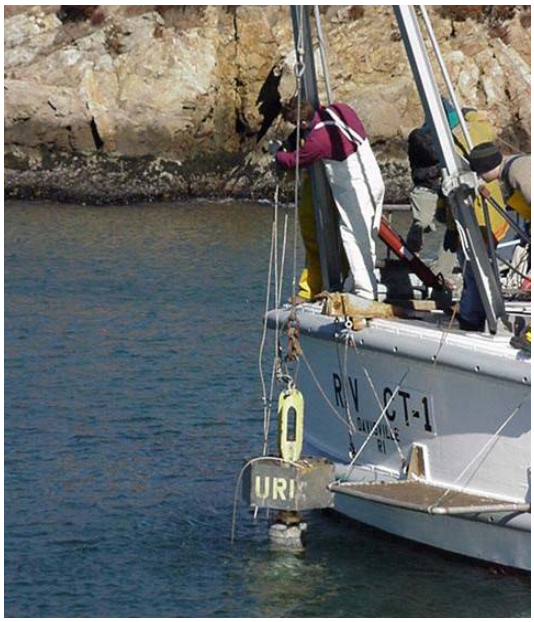

Figure 4.3. Sediment sampling at Fort Wetherill using
the URI Large-Diameter Gravity Corer.

Based on the results of index tests on sediment samples, the site consists of layers of black organics, silty sand, fine to medium sand, coarse to fine gravel and weathered rock.

Two steel reinforced plastic (PPI) piles and two concrete-filled fiberglass plastic piles (FRP) were installed along the northern side of the pier, as shown in Figure 4.2b. The piles were 40 feet in length. In addition to the composite piles, timber (greenheart) piles were installed elsewhere on the project site.

4.3 Pile Installation

Narragansett Dock Works installed the composite piles on February 26-27, 2004 using a small vibratory hammer. For each pile, an existing greenheart timber pile was first driven, as shown in Figure 4.4, in advance of the composite pile in order to create a pilot hole for the permanent composite pile. This was done because the contractor experienced difficult driving on a previous job at this site within the top 1m to 1.5m (3 ft to 5 ft) from the mudline, which was attributed to either eroded/spalled materials from the dock itself or to new gravel/sand placed at the mudline to replace eroded sediments. Following the predriving, the composite piles were installed to an embedment depth of approximately 19 ft (5.8m).

The FRP pile required special handling during pickup and movement into driving position in order to minimize tensile stresses in the pile. The manufacturer recommends using several pickup points to minimize bending; however the contractor chose to fasten a W8x28 steel section to the FRP pile, as shown in Figure 4.5. Both the steel and FRP piles were lifted together until they were in the vertical position. This method appeared to be very effective in preventing bending of the FRP pile. The PPI piles did not warrant any special handling requirements and were moved across the site using a small rubber tire front-loader, Bobcat.

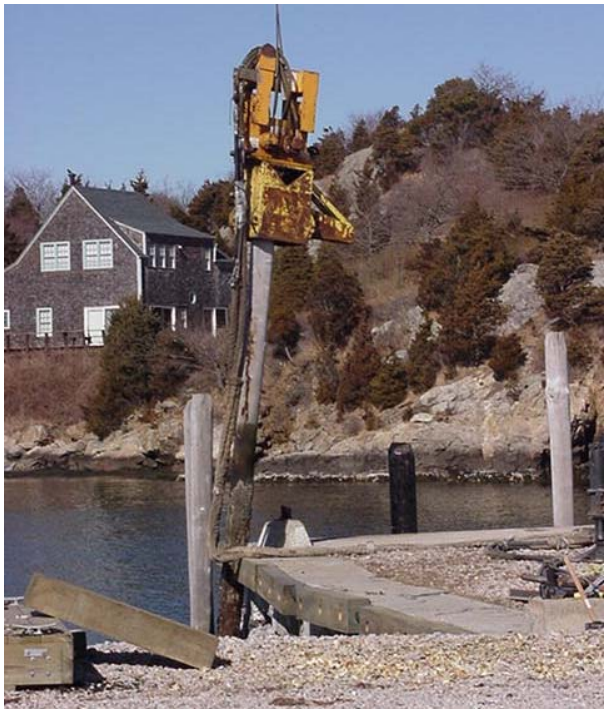

Figure 4.4. Predriving using a Greenheart timber pile.

Figure 4.5. Use of W8x28 section to prevent bending of FRP pile during handling.

Upon visual inspection of the piles after installation was complete, damage to the top portion of the piles was clearly noticeable. The PPI pile, as shown in Figure 4.6a, experienced damage due to friction heating caused by the clamping of the vibratory hammer to the pile itself. The FRP pile, as shown in Figure 4.6b, experienced damage to the fiberglass exterior due to friction and slippage caused by the clamping of the vibratory hammer during installation.

(a) (b)

Figure 4.6. Damage to the a.) PPI pile and b.) FRP pile during installation.

4.4 Field Testing Methodology

4.4.1 Test Configuration

The fender piles were laterally impacted using a ship called the Beavertail from Jamestown, RI. The vessel, which was built by the U.S. Army in 1940 for mine distribution, has an overall length of 64ft (19.51m), a beam of 18ft (5.49m), and a draft of 7ft (2.13m). The vessel was originally designed for a displacement of 68 tons (605 kN), however, the current displacement is larger considering recent installation of larger fuel tanks and ballast. The estimated displacement is approximately 85 tons (756 kN) (Fred Pease, URI Ocean Engineering ship captain and former owner of the Beavertail, personal communication). The impact loads were calculated using a kinetic energy formulation based on the estimated mass and approach velocity of the vessel.

The piles were instrumented with acceleration and displacement transducers to measure their dynamic response to impact, as shown in Figure 4.7. The displacements at four locations along the pile were determined by double integrating the obtained acceleration signals. The accuracy of the integration was assessed at one location by comparing the integrated accelerometer displacements with displacement measurements obtained by a separate displacement transducer.

In order to perform the impact test, the boat was oriented perpendicular to the test pile, as shown in Figure 4.8. Dock lines were attached to an adjacent pier to maintain the orientation of the boat such that its stern would strike the pile head-on. At approximately 10 to 15 ft from the pile, the boat was put in gear and accelerated to a velocity of about 0.4 to 0.8 ft/sec (0.13 to 0.25 m/sec). A few feet before impact, the boat was put into neutral allowing the boat to drift into the fender pile. During impact, the acceleration time history was recorded using acceleration transducers mounted at four locations along the pile. A total of 6 impact tests were performed on the PPI piles and 9 tests were performed on the FRP piles.

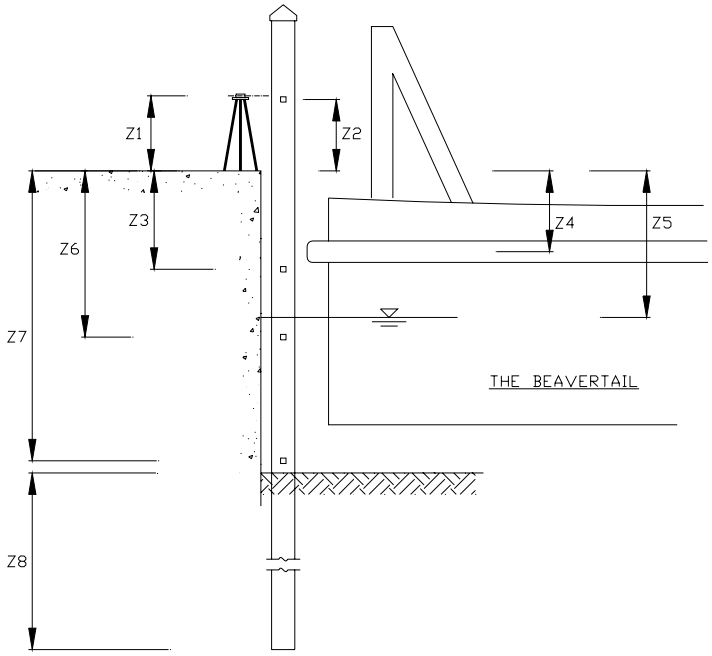

	Description	FRP Pile	PPI Pile
Z1	Deck to Displacement Transducer	3'-4"	3'-7"
Z2	Deck to Accelerometer 1	3'-6"	3'-6"
Z3	Deck to Accelerometer 2	4'-7"	4'-9"
Z4	Deck to Impact Location	3'-9"	3'-7"
Z5	Deck to Water Level	6'-8"	6'-8"
Z6	Deck to Accelerometer 3	7'-3"	7'-2"
Z7	Deck to Accelerometer 4	13'-10"	13'10"
Z8	Embedment Length	19'-0"	19'-0"

Figure 4.7. Cross-section of test layout, including location of instrumentation.

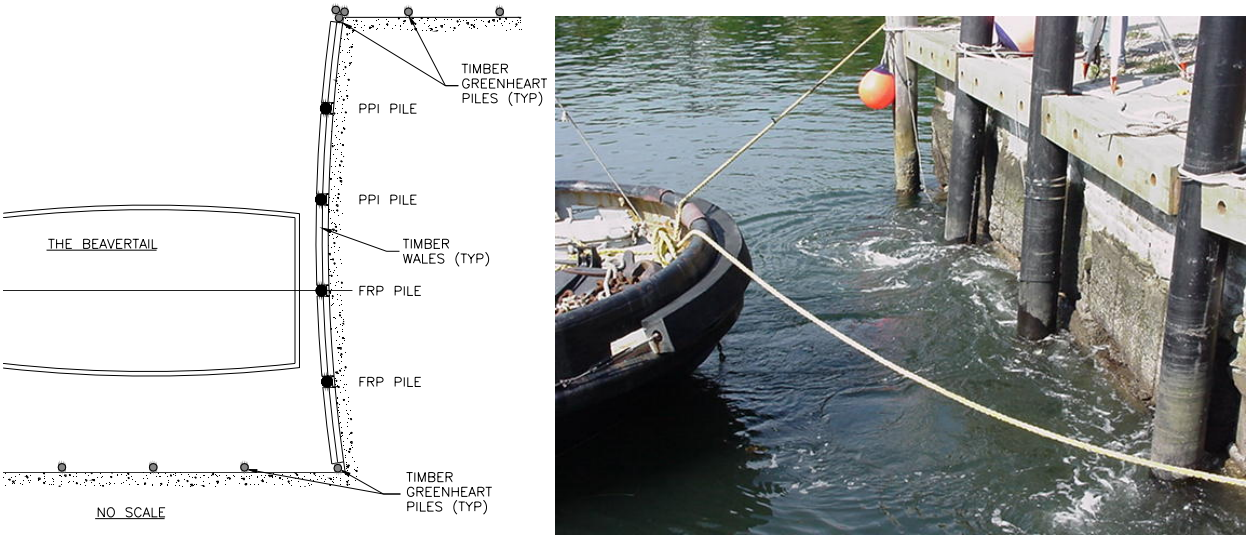

Figure 4.8. Setup for impact load tests.

4.4.2 Instrumentation

Two different types of accelerometers and one acoustic displacement transducer were used in this study. The accelerometers, shown in Figure 4.9, are manufactured by Kistler Instrument Corporation (models 8305A and 8310A). The acceleration transducers were fastened to the face of the composite piles at various vertical positions to measure the dynamic response of the composite piles.

(a) (b)

Figure 4.9. a.) Kistler 8305A differential (top) and 8310A single-ended (bottom) accelerometers, and b.) mounting an accelerometer on the pile (Kistler, 2004).

Prior to performing the field experiments, all four accelerometers were calibrated separately employing the same procedure. Each accelerometer was placed in three orientations that corresponded to three different values of acceleration. The positive (horizontal, face up) position corresponds to an acceleration of 1 g. The vertical position and the negative (horizontal, face down) position correspond to accelerations of 0 and –1 g.

Displacements were measured at one point on the piles using a Massa M-5000 Smart Ultrasonic Displacement Transducer, as shown in Figure 4.10. The transducer was mounted on a tripod and positioned in close vertical proximity to the uppermost acceleration transducer (Figure 4.7) in order to provide a redundant measurement with one of the accelerometers.

Data was acquired using a laptop personal computer with a National Instruments data acquisition card and the program LabView6.

Figure 4.10. Massa M-5000 Smart Ultrasonic Sensor (Massa, 1998).

4.5 Data Processing

Processing of the raw accelerometer and displacement data included filtering the signals, double integration of the accelerations, and plotting the results. This was done by Jason Ressler of the URI Ocean Engineering Department using the program MATLAB. The processing script is shown in Appendix A.

The accelerometers are insensitive to transverse motion; that is, the transducers only pick up accelerations that are normal to the face of the instrument. Because the piles were installed with a slight batter, it was not possible to mount the accelerometers perfectly vertical. This introduced a small component of gravity acting normal to the face of each instrument to the recorded signals. Two components of each signal exist: a vertical component due to gravity and the horizontal component due to the impact force. The ratio of the vertical to horizontal acceleration components is directly dependant on the mounting angle of the accelerometer, with respect to the vertical.

In order to decouple the acceleration signal from gravity, an acceleration offset, determined by using the acceleration data during the at-rest state, was applied to the data. For each accelerometer, the same offset was used throughout. This assumes that the accelerometer angle on the pile remains constant throughout its motion, which is reasonable during the early stages of impact. For future tests, it is recommended that an inclinometer and accelerometer assembly or a gimbaled accelerometer be used to accurately segregate the horizontal component of acceleration from the entire signal.

Each signal was then filtered using a low pass filter. The filter was applied prior to the integration in order to minimize the propagation of errors from the signal noise. An order 1 Butterworth filter with a non-dimensional cutoff of 0.05 was used. At a sampling frequency of 200 Hz, this cutoff corresponds to a 10 Hz low pass filter. The 10 Hz cutoff frequency was chosen based on a review of the power spectral density of the signal. The majority of the noise in the signals occurred around 80 Hz and additional peaks were found at approximately 20 to 40 Hz. Assuming no impact ever exceeded 10 seconds, which can be verified by analyzing the acceleration time history records, this method will accurately filter unwanted noise without affecting the dynamic impact signal. Filtered and unfiltered acceleration signals from impact test 4 on the FRP pile are presented in Figure 4.11. An example of the filtered acceleration data, for the same test, with the displacement data found using the displacement transducer is presented in Figure 4.12. Acceleration and displacement data for all the tests are included in Appendix B.

Once the calibrations, corrections and filtering were performed, the acceleration data were double integrated in order to compute the pile displacement at each location. A discrete measurement trapezoidal rule was used for the integration. The equations used for the calculation of velocity (first integration) and displacement (second integration) from the measured acceleration data are presented below and typical results of the integration are shown in Figure 4.13. Equation 4.1 illustrates numerically that the velocity at the time between two successive acceleration measurements is the cumulative area under the acceleration-time curve.

$$v_t = \frac{1}{2 f_s}(a_t + a_{t-1}) + v_{t-1} \qquad \text{(Eq. 4.1)}$$

$$s_t = \frac{1}{2 f_s}(v_t + v_{t-1}) + s_{t-1} \qquad \text{(Eq. 4.2)}$$

where:

a_t = acceleration at present time increment, ft/s^2
a_{t-1} = acceleration at previous time increment, ft/s^2
f_s = sampling frequency, Hz
s_t = displacement at present time increment, ft
s_{t-1} = displacement at previous time increment, ft
v_t = velocity at present time increment, ft/sec
v_{t-1} = velocity at previous time increment, ft/sec

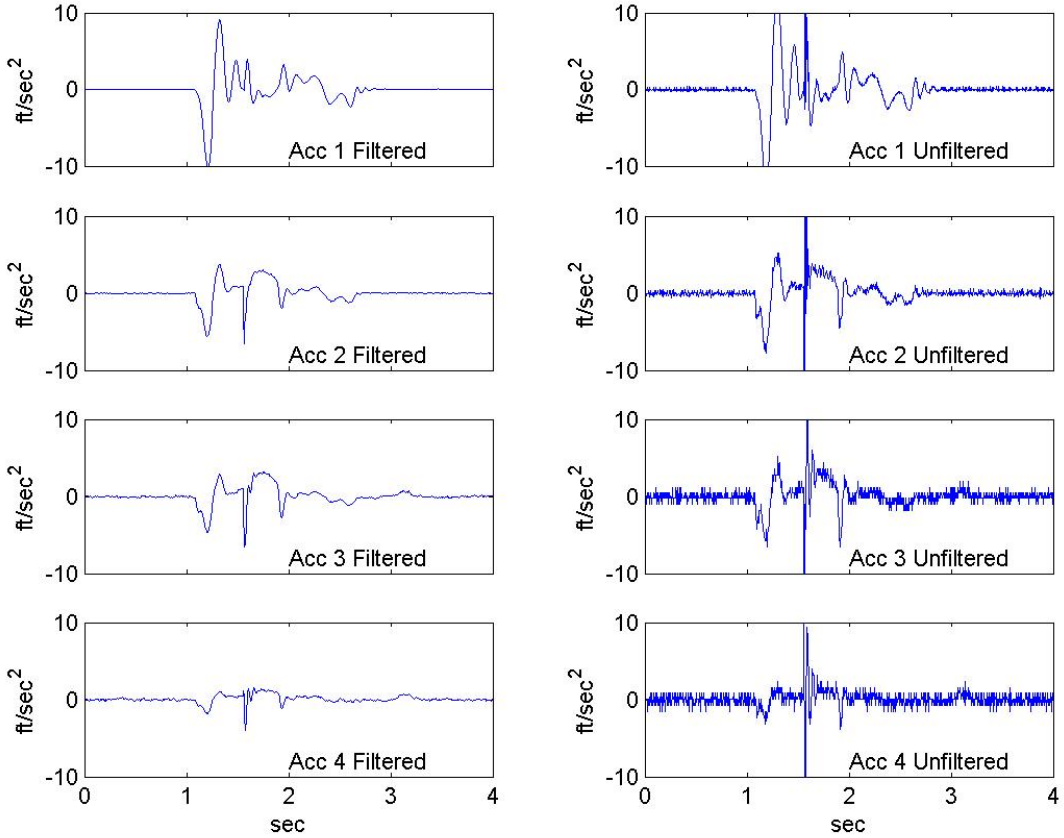

Figure 4.11. Filtered and unfiltered acceleration signals from FRP Pile impact test 4.

The displacements obtained from double integrating the acceleration signal from the uppermost acceleration transducer were then compared to the displacements obtained from the displacement transducer. Figure 4.13 shows excellent agreement between the measured and calculated displacement for most of the time history. However, the calculated displacement incorrectly increases linearly at the end of each signal. This error is addressed in section 4.6.1.

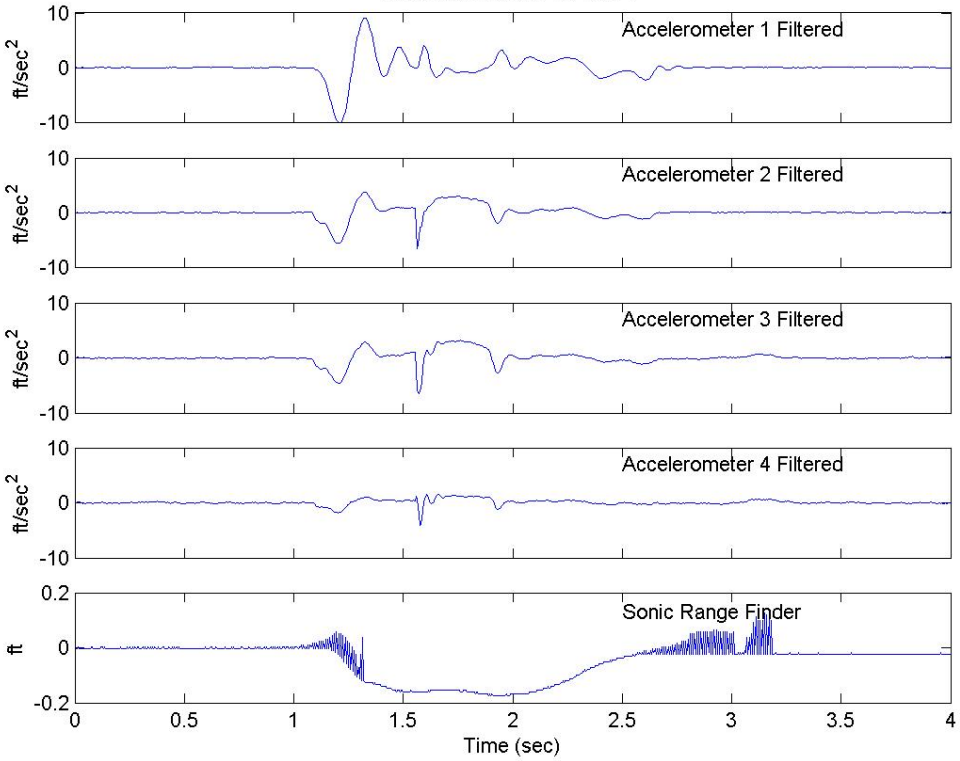

Figure 4.12. Filtered acceleration and displacement graphs for FRP pile impact Test 4.

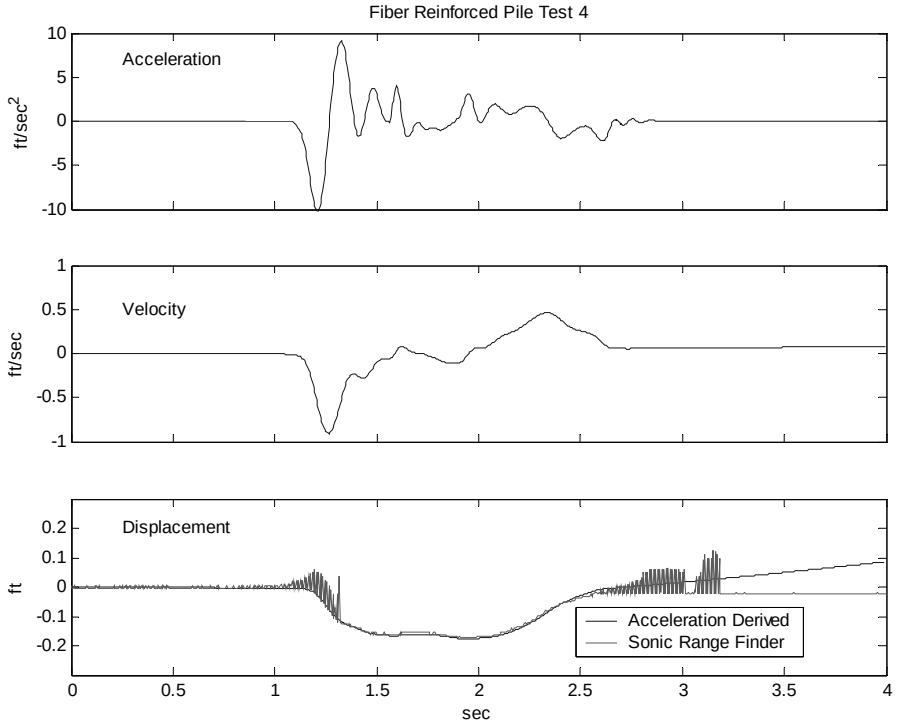

Figure 4.13. Acceleration, velocity and displacement response for FRP pile impact test 4.

4.6 Dynamic Response of Impact Tests

The acceleration and displacement response of the FRP and plastic pile is shown in Figure 4.14. Accelerometer 1 was located above the bulkhead and the elastomeric bumper, accelerometer 2 was located at the point of impact, accelerometer 3 was located below the point of impact and below the water surface, and accelerometer 4 was located at the mudline. Both tests showed that the maximum displacement occurred at accelerometer 1, and that the displacements at accelerometers 1 and 2 were in the direction away from the vessel. At accelerometers 3 and 4, however, the displacements were in the direction of the vessel. This means that there was some rotation in addition to translation and bending of the piles during impact.

There was significantly less acceleration and displacement observed in the PPI pile at accelerometers 2, 3, and 4 than for the FRP pile. Unfortunately, this is due to a large stone block that protrudes from the pier and touches the PPI pile below the water line. The presence of this block acted as a pin support and affected the displacement of the pile. It appeared that both PPI piles were placed against this block when they were installed. This reduces the ability of the PPI piles to bend during impact and reduces the overall effectiveness of the fender system.

The maximum displacements from each impact test and instrument are presented in Table 4.2. Since these displacements do not show a linear increase with respect to distance from the mud line, it is concluded that the piles were in fact bending during impact.

Table 4.2. Maximum displacements for FRP and PPI pile tests for each accelerometer (see Figure 4.7 for location).

		Maximum Displacement				
Pile Type	**Test Number**	**Acc 1**	**Acc 2**	**Acc 3**	**Acc 4**	**Sonic**
		(ft)	(ft)	(ft)	(ft)	(ft)
FRP	1	0.129	0.090	0.059	0.002	0.124
FRP	2	0.154	0.120	0.097	0.029	0.145
FRP	3	0.162	0.129	0.110	0	0.153
FRP	4	0.167	0.178	0.170	0.029	0.172
FRP	5	0.148	0.128	0.086	NA	0.145
FRP	6	0.147	0.118	0.070	NA	0.143
FRP	7	0.133	0.118	0.092	NA	0.153
FRP	8	0.161	0.127	0.090	0	0.157
FRP	9	0.150	0.126	0.097	0.018	0.149
PPI	1	0.085	0.032	0.036	NA	0.119
PPI	2	0.107	0.044	0.002	0	0.127
PPI	3	0.128	0.032	0.096	0	0.139
PPI	4	0.140	0.046	0.062	0	0.153
PPI	5	0.167	0.046	0.019	0	0.198
PPI	6	0.209	0.123	0.064	0.001	0.181

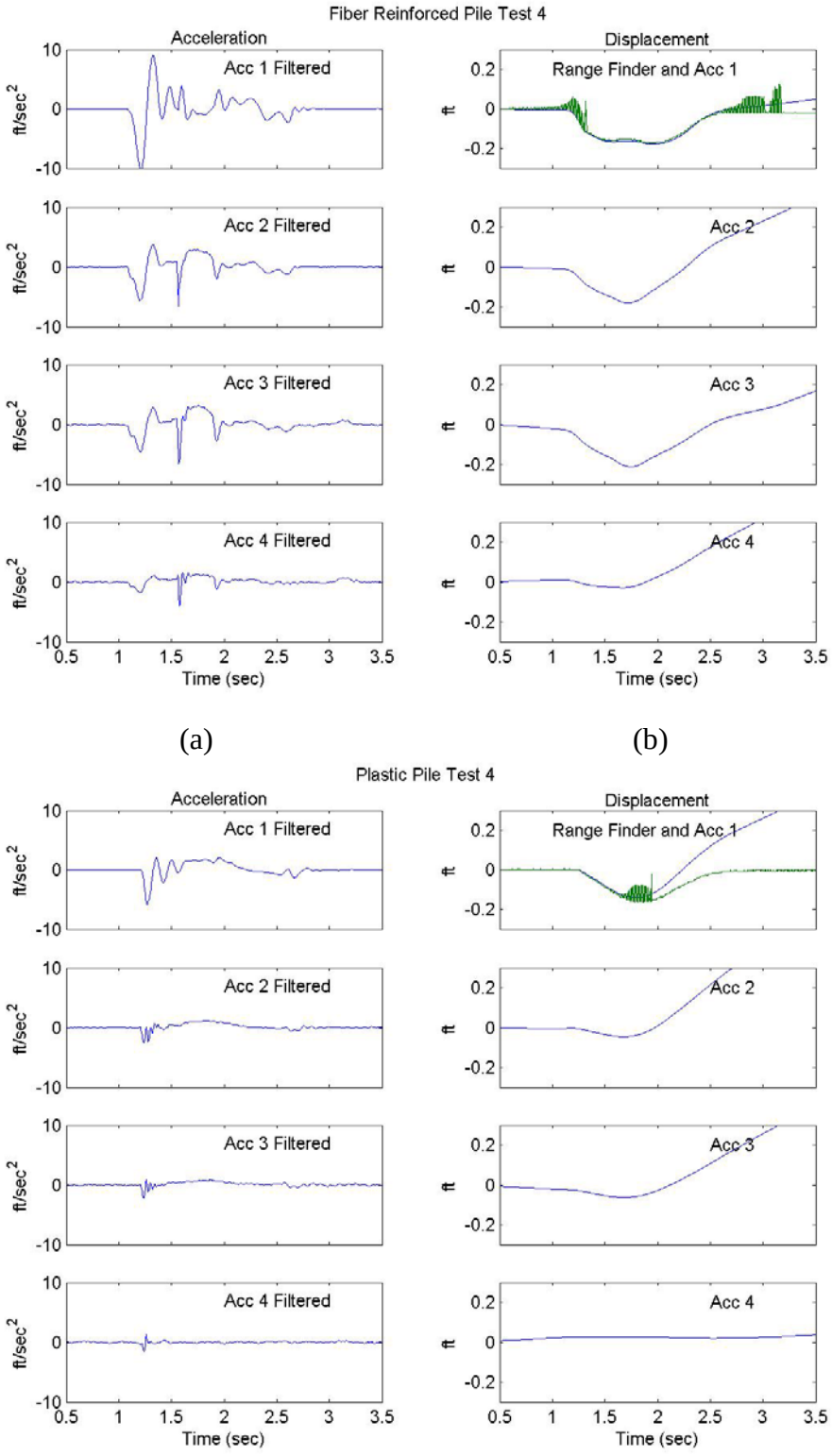

Figure 4.14. Acceleration and displacement response of the FRP pile (a and b) and the plastic pile (c and d) during impact.

4.6.1 Corrections to Accelerometer Data

As discussed in Section 4.5, the displacement time histories of the pile were obtained through double integration of the accelerometer signals. Pile displacements were also measured directly using a sonic range finder to obtain the data shown in Figures 4.13 and 4.14. It is clear from the sonic data that the pile starts at zero displacement, reaches a maximum value and returns back to zero. However, as shown in the figures, the displacements obtained through integration of the accelerometers do not return to zero at the end of impact, but rather increase unbounded. Also velocity signals integrated from the accelerometers also show a non-zero "residual" velocity even after the pile has stopped moving.

Since integration is the summation of the areas under a given function, a non-zero velocity at the end of the test would indicate that the sum of the positive and negative areas under the acceleration signal are not equal. Further analysis of the accelerometer data indicates that this discrepancy was caused by rotation of the accelerometers during pile displacement which were inadvertently introducing some gravitational acceleration into the acceleration signals. For example, when the accelerometer is positioned vertically the accelerometer reads zero acceleration, whereas 1 g is registered when it is rotated to the horizontal position. Therefore, the raw acceleration signals were corrected to remove the gravitational effects caused by rotation of the instrument.

The correction was performed by subtracting a half sine wave correction function from the acceleration time history. A half sine was selected because it mimics the shape of the displacement time history and hence the rotation of the accelerometer. Examples of a typical acceleration signal and correction function for FRP Test 1 (ACC 2) are shown in Figure 4.15. First, the period of the correction function (bottom of figure) is adjusted to match the duration of the acceleration signal (top). Second, the amplitude of the correction function is modified until the velocity at the end of the test is zero. The velocity and displacement time histories after the correction is made are shown in Figure 4.16, both of which show zero values at the end of the test.

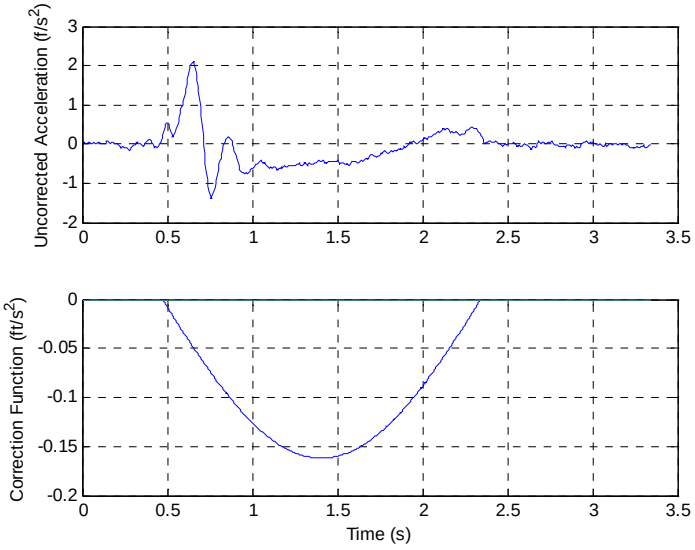

Figure 4.15. Acceleration signal (top) and correction function (bottom).

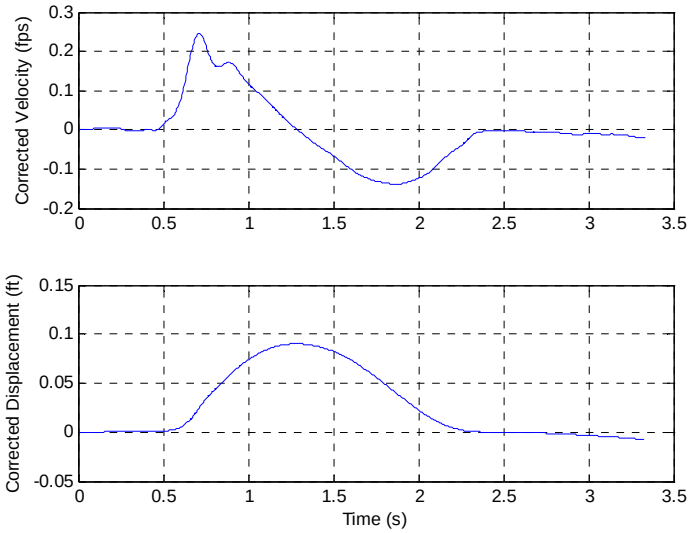

Figure 4.16. Corrected velocity (top) and displacement (bottom) time histories.

4.6.2 Evaluation of Fender Pile Stiffness Using Kinetic Energy Approach

The response of any system to a dynamic load depends on the stiffness and damping characteristics of the system. In the design of fendering systems, the objective is to minimize vessel impact stresses and reduce vessel accelerations within allowable limits. The impact tests performed in the field were used to estimate the dynamic stiffness of the fender piles assuming a perfectly elastic system. The damping characteristics of the composite piles were not evaluated.

If it is assumed that the fender pile system is a perfectly elastic system, then during impact the initial kinetic energy of the boat is transferred to potential energy stored in the fender pile system. The kinetic energy of the boat can be estimated using Equation 4.3 (Gaythwaite 2004).

$$E = \frac{\Delta}{2g} V_n^{\,2} \qquad \text{(Eq. 4.3)}$$

where:

E	=	Kinetic energy of vessel,
Δ	=	Vessel displacement,
g	=	Acceleration of gravity,
V_n	=	Velocity of vessel normal to pile.

As a first order approximation, additional vessel masses from hydrodynamic effects have been neglected. The maximum reaction force on a perfectly elastic fender pile can be calculated using Equation 4.4 (Gaythwaite 2004).

$$R_{\max} = \frac{2E}{\delta_{\max}} \qquad \text{(Eq. 4.4)}$$

where:

R_{max} =Maximum reaction force,

δ_{max} =Maximum pile displacement.

The equivalent spring constant, K, for the fender pile can be calculated using Equation 4.5.

$$K = \frac{R_{max}}{\delta_{max}} \quad \text{(Eq. 4.5)}$$

A summary of average values for vessel velocity, vessel energy, maximum displacement, maximum reaction force, and pile stiffness are summarized in Table 4.3. In principle, these values of stiffness can be used to design future fender pile systems with the composite piles. However, the stiffness of the PPI pile system is too high because of the restraint caused by the stone block described above, and that value is not representative of typical conditions.

Table 4.3. Summary of average vessel and fender pile parameters.

Pile Type	**V_n** (ft/sec)	**E** (kip-ft)	**δ_{max}** (ft)	**R_{max}** (kip)	**K** (kip/ft)
FRP	0.56	0.83	1.36	1.22	0.90
PPI	0.69	1.26	0.64	3.93	6.14

5.0 A New Dynamic Model for Analysis and Design of Fender Piles

The kinetic energy approach described in section 4.6.2 is the most commonly used method in the design of fender systems (Gaithewaite 2004). In this approach, the kinetic energy of a berthing vessel is compared to the energy absorbing capacity of the fender system, and the fender elements are selected or configured to limit stresses below allowable criteria. The energy absorbing capacity of a fender element is evaluated by calculating the area under the static force verses displacement curve. Energy concepts have been adopted for the analysis of free-standing fender piles (Reese et al. 1970), concrete fender piles (Li and Ramakrishnan 1971), and timber fender piles (USACE 1983).

Since the energy capacity of fender piles are derived from static tests or analyses, the kinetic energy method does not consider the energy dissipated during vessel impact. Energy dissipation should be considered in design because it has the effect of reducing the forces on the vessel and pile. The first half of this chapter presents a description of a dynamic model that is derived for a typical fender pile configuration. In this model, the fender pile and impacting vessel are treated as a freely vibrating multi-degree of freedom structure with lumped masses. The second half of the chapter presents a comparison of the field impact tests performed on the FRP composite fender pile and the results of the dynamic model.

5.1 Description of the Dynamic Model

The dynamics of a vessel impacting a fender pile are best illustrated by the simple model shown in Figure 5.1. In this model the pile is represented by a frictionless mass (M_p) attached to a spring and a dashpot and the approaching vessel is represented by a second frictionless mass (M_v) having an initial velocity V_{vo}. The spring represents the stiffness and the dashpot represents the energy dissipated in the system. Before impact (Figure 5.1a) the pile mass is in static equilibrium with zero displacement and zero velocity. At impact (Figure 5.1b) the vessel mass becomes coupled to the pile mass and as the spring is compressed the vessel mass is slowed eventually stopping at the point of maximum displacement (Figure 5.1c). The strain energy stored in the spring pushes the vessel back to the equilibrium point where it becomes decoupled from the pile (Figure 5.1d). The velocity of the vessel at the point when it leaves the pile (V_{vf}) is less than the impact velocity due to the dissipated energy.

The dynamic motion of the fender pile system is therefore analogous to a freely vibrating system for ½-cycle which has zero initial displacement and an instantaneous velocity. For a more accurate representation of the various parameters involved, a multi-degree of freedom approach can be followed in which the structure is modeled as a system of lumped masses with stiffness and damping. A schematic of the dynamic fender pile model used in this study is shown in Figure 5.2. The pile model consists of nine lumped masses positioned along a flexible beam: one at the upper support at deck level (m_1), one at the vessel impact location (m_2), two along the submerged part of the pile (m_3 and m_4), and the remaining five positioned over the embedded portion of the pile (m_5 through m_9). Linear springs are used to model the stiffness of the soil and the rubber fender which provides support near the top of the pile. The system has 18 degrees of freedom including one translation and one rotation at each node.

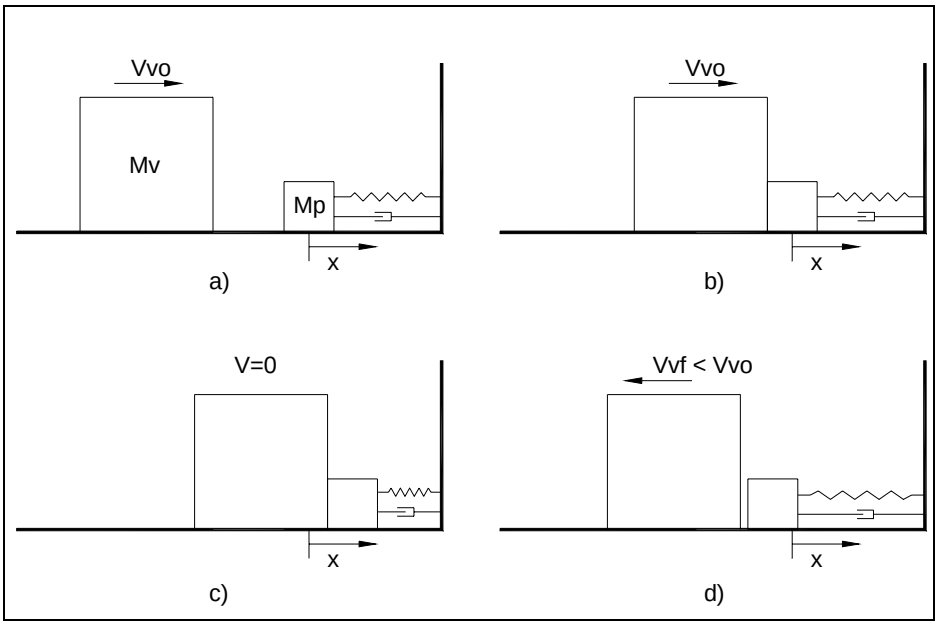

Figure 5.1. Schematic of the dynamics of a vessel impacting a fender pile: (a) prior to impact, (b) at time of impact, (c) after impact, and (d) after decoupling.

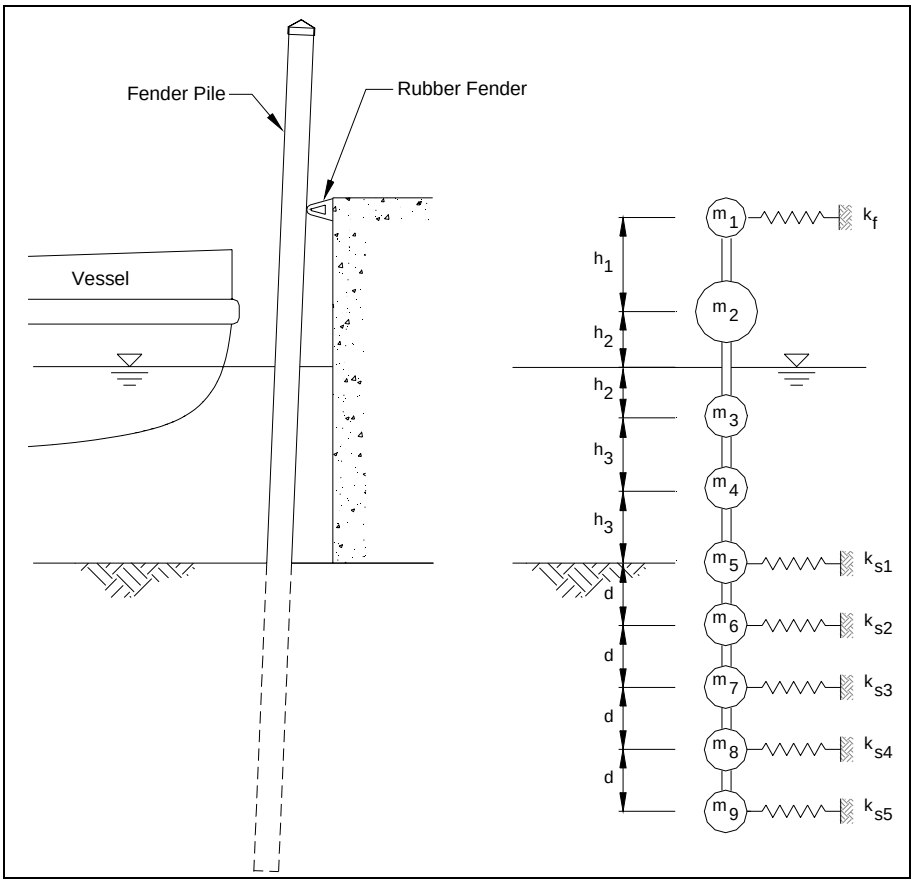

Figure 5.2. Schematic of the dynamic fender pile model.

In a single degree of freedom system, the equation of motion governing the free response of the system is based on Newton's second law defined by the following partial differential equation

$$m\ddot{x} + c\dot{x} + kx = 0 \qquad \text{(Eq. 5.1)}$$

Where *m*, *c* and *k* are the mass, damping, and stiffness, and $\ddot{x}$, $\dot{x}$, and *x*, are the acceleration, velocity, and displacement. For an N-degree of freedom system there is a system of N coupled differential equations having N number of modes and N number of natural frequencies. A multi-degree of freedom system can be expressed in terms of its modal coordinates whose equation of motion is of similar form to the single degree of freedom system (Chopra 2000)

$$M_n\ddot{q}_n + C_n\dot{q}_n + K_n q_n = 0 \qquad \text{(Eq. 5.2)}$$

Where,

$$M_n = \bar{\phi}_n^T \mathbf{m} \bar{\phi}_n, \qquad C_n = \bar{\phi}_n^T \mathbf{c} \bar{\phi}_n, \quad K_n = \bar{\phi}_n^T \mathbf{k} \bar{\phi}_n$$

The modal quantities q_n, $\dot{q}_n$, and $\ddot{q}_n$ in Equation (5.2) are analogous to x, $\dot{x}$, and $\ddot{x}$ in the 1-D equation of motion. The mode shapes $\bar{\phi}_n$ are vectors that describe the deflected shapes of the lumped masses for each mode of oscillation. Equation (5.2) can be re-written by dividing through by M_n and simplifying to obtain the following expression

$$\ddot{q}_n + 2\zeta_n\omega_n\dot{q}_n + \omega_n^2 q_n = 0 \qquad \text{(Eq. 5.3)}$$

The solution to Equation (5.3) is of similar form to the solution of a SDOF system given by

$$q_n(t) = \left(q_n(0)\cos\omega_{nd}t + \left(\frac{\dot{q}_n(0) + \zeta_n\omega_n q_n(0)}{\omega_{nd}} \right)\sin\omega_{nd}t \right)\exp\left(-\zeta_n\omega_n t\right) \qquad \text{(Eq. 5.4)}$$

Where,

$$q_n(0) = \frac{\bar{\phi}_n^T \mathbf{m}\bar{x}(0)}{M_n}, \qquad \dot{q}_n(0) = \frac{\bar{\phi}_n^T \mathbf{m}\dot{\bar{x}}(0)}{M_n}$$

The variables $q_n(0)$ and $\dot{q}_n(0)$ define the initial conditions of the system given an initial displacement vector $\bar{x}(0)$ and an initial velocity vector $\dot{\bar{x}}(0)$. Since the pile is initially at the equilibrium position (i.e. $\bar{x}(0) = 0$), Equation (5.4) simplifies to the following

$$q_n(t) = \left[\frac{\dot{q}_n(0)}{\omega_{nd}}\sin\omega_{nd}t \right]\exp\left(-\zeta_n\omega_n t\right) \qquad \text{(Eq. 5.5)}$$

The mass at the vessel impact point (m_2 in Figure 5.2) is assumed to have an instantaneous velocity equal to the vessel velocity while all other masses have initial velocities of zero. The damped natural frequency of each mode of oscillation (ω_{nd}) is a function of the undamped natural frequency (ω_n) and the damping ratio (ζ_n) given by

$$\omega_{nd} = \omega_n \sqrt{1 - \zeta_n^{\,2}} \qquad \text{(Eq. 5.6)}$$

The undamped natural frequency of each mode (ω_n) is determined by solving the characteristic equation

$$\det\left[\mathbf{k} - \omega_n \mathbf{m}\right] = 0 \qquad \text{(Eq. 5.7)}$$

And the corresponding mode shapes ($\bar{\phi}_n$) can be evaluated from the following equation

$$\left[\mathbf{k} - \omega_n \mathbf{m}\right]\bar{\phi}_n = 0 \qquad \text{(Eq. 5.8)}$$

Note that ω_n and $\bar{\phi}_n$ can also be evaluated simultaneously using the eigenvalue problem function in the program Matlab. The time varying displacements are evaluated by multiplying Equation (5-5) by the corresponding mode shape and summing the responses of each mode

$$\bar{x}(t) = \sum_{n=1}^{9} \bar{\phi}_n \left[\frac{\dot{q}_n(0)}{\omega_{nd}} \sin \omega_{nd} t \right] \exp\left(-\zeta_n \omega_n t\right) \qquad \text{(Eq. 5.9)}$$

Differentiation of Equation (5.9) with respect to time also yields the velocity of the system

$$\dot{\bar{x}}(t) = \sum_{n=1}^{9} \bar{\phi}_n \left[\dot{q}_n(0) \cos \omega_{nd} t - \frac{\dot{q}_n(0) \zeta_n \omega_n}{\omega_{nd}} \sin \omega_{nd} t \right] \exp\left(-\zeta_n \omega_n t\right) \qquad \text{(Eq. 5.10)}$$

For design it is of interest to determine the forces acting on the pile from the impacting vessel. The equivalent static force acting at the impact point (F_2) can be evaluated from the product of the stiffness matrix and calculated displacements

$$F_2(t) = \left[\mathbf{k} \cdot \bar{x}(t)\right]_{i=2} \qquad \text{(Eq. 5.11)}$$

Likewise, the force applied to the pier structure through the fender support (F_1) can be determined from the spring constant and displacements at the uppermost node

$$F_1(t) = k_f \cdot x(t)_{i=1} \qquad \text{(Eq. 5.12)}$$

And the maximum moment in the pile at any given time under the given pile configuration can be readily obtained

$$M_{\max}(t) = F_1(t) \cdot h_1 \qquad \text{(Eq. 5.13)}$$

To determine the dynamic response of the fender pile, appropriate mass and stiffness matrices and damping ratio must be established. These parameters are discussed in detail in subsequent sections.

5.1.1 Mass Matrix

As shown in Figure 5.2, the fender pile model consists of 9 lumped masses (m_1 through m_9) each having 18 degrees of freedom including 9 translation and 9 rotation. It is anticipated that the pile inertia will be primarily translational, and thus the masses associated with rotation are neglected to yield a diagonal mass matrix (**m**) where the term m_{ii} in the matrix is defined as

$$m_{ii} = m_i \qquad \text{(Eq. 5.14)}$$

The mass of the pile itself is distributed among the lumped masses in proportion to the spacing between nodes. In addition to the pile mass, mass m_2 also includes the vessel mass and vessel hydrodynamic added mass. Masses m_3 and m_4 also include the hydrodynamic added mass of the pile moving laterally through the water column. These parameters will be quantified for the impact test discussed in the next section.

5.1.2 Stiffness Matrix

The stiffness matrix provides the restoring force in the dynamic system and was evaluated for the fender pile using the direct stiffness method (e.g. Leet 1988). A typical term k_{ij} within the stiffness matrix **k** is determined as the force at degree of freedom i due to a unit displacement at j when all other displacements are zero. Each term in the stiffness matrix was derived for the 18 degrees of freedom for the model shown in Figure 5.2 yielding an 18 by 18 matrix. To be consistent with the size of the 9 by 9 mass matrix but still include rotational stiffness, the stiffness matrix is condensed by first partitioning the 18 by 18 matrix as follows:

$$\mathbf{k} = \left[\begin{array}{c|c} \mathbf{k}_{tt} & \mathbf{k}_{to} \\ \hline \mathbf{k}_{ot} & \mathbf{k}_{oo} \end{array}\right] \qquad \text{(Eq. 5.15)}$$

And then substituting the submatricies into the following expression (Chopra 2000)

$$\mathbf{k} = \mathbf{k}_{tt} - \mathbf{k}_{to}\mathbf{k}_{oo}^{-1}\mathbf{k}_{ot} \qquad \text{(Eq. 5.16)}$$

Where,

$$\mathbf{k}_{tt} = \begin{bmatrix}
\frac{12EI}{h_1^3}+k_f & \frac{-12EI}{h_1^3} & 0 & 0 & 0 & 0 & 0 & 0 & 0 \\
\frac{-12EI}{h_1^3} & \frac{12EI}{h_1^3}+\frac{3EI}{2h_2^3} & \frac{-3EI}{2h_2^3} & 0 & 0 & 0 & 0 & 0 & 0 \\
0 & \frac{-3EI}{2h_2^3} & \frac{3EI}{2h_2^3}+\frac{12EI}{h_3^3} & \frac{-12EI}{h_3^3} & 0 & 0 & 0 & 0 & 0 \\
0 & 0 & \frac{-12EI}{h_3^3} & \frac{24EI}{h_3^3} & \frac{-12EI}{h_3^3} & 0 & 0 & 0 & 0 \\
0 & 0 & 0 & \frac{-12EI}{h_3^3} & \frac{12EI}{h_3^3}+\frac{12EI}{d^3}+k_{S1} & \frac{-12EI}{d^3} & 0 & 0 & 0 \\
0 & 0 & 0 & 0 & \frac{-12EI}{d^3} & \frac{24EI}{d^3}+k_{S2} & \frac{-12EI}{d^3} & 0 & 0 \\
0 & 0 & 0 & 0 & 0 & \frac{-12EI}{d^3} & \frac{24EI}{d^3}+k_{S3} & \frac{-12EI}{d^3} & 0 \\
0 & 0 & 0 & 0 & 0 & 0 & \frac{-12EI}{d^3} & \frac{24EI}{d^3}+k_{S4} & \frac{-12EI}{d^3} \\
0 & 0 & 0 & 0 & 0 & 0 & 0 & \frac{-12EI}{d^3} & \frac{24EI}{d^3}+k_{S5}
\end{bmatrix}$$

$$\mathbf{k}_{to} = \begin{bmatrix}
\frac{6EI}{h_1^2} & \frac{6EI}{h_1^2} & 0 & 0 & 0 & 0 & 0 & 0 & 0 \\
\frac{-6EI}{h_1^2} & \frac{3EI}{2h_2^2}-\frac{6EI}{h_1^2} & \frac{3EI}{2h_2^2} & 0 & 0 & 0 & 0 & 0 & 0 \\
0 & \frac{-3EI}{2h_2^2} & \frac{6EI}{h_3^2}-\frac{3EI}{2h_2^2} & \frac{6EI}{h_3^2} & 0 & 0 & 0 & 0 & 0 \\
0 & 0 & \frac{-6EI}{h_3^2} & 0 & \frac{6EI}{h_3^2} & 0 & 0 & 0 & 0 \\
0 & 0 & 0 & \frac{-6EI}{h_3^2} & \frac{6EI}{d^2}-\frac{6EI}{h_3^2} & \frac{6EI}{d^2} & 0 & 0 & 0 \\
0 & 0 & 0 & 0 & \frac{-6EI}{d^2} & 0 & \frac{6EI}{d^2} & 0 & 0 \\
0 & 0 & 0 & 0 & 0 & \frac{-6EI}{d^2} & 0 & \frac{6EI}{d^2} & 0 \\
0 & 0 & 0 & 0 & 0 & 0 & \frac{-6EI}{d^2} & 0 & \frac{6EI}{d^2} \\
0 & 0 & 0 & 0 & 0 & 0 & 0 & \frac{-6EI}{d^2} & \frac{6EI}{d^2}
\end{bmatrix}$$

$$\mathbf{k}_{ot} = \begin{bmatrix}
\frac{6EI}{h_1^2} & \frac{-6EI}{h_1^2} & 0 & 0 & 0 & 0 & 0 & 0 & 0 \\
\frac{6EI}{h_1^2} & \frac{3EI}{2h_2^2}-\frac{6EI}{h_1^2} & \frac{-3EI}{2h_2^2} & 0 & 0 & 0 & 0 & 0 & 0 \\
0 & \frac{3EI}{2h_2^2} & \frac{6EI}{h_3^2}-\frac{3EI}{2h_2^2} & \frac{-6EI}{h_3^2} & 0 & 0 & 0 & 0 & 0 \\
0 & 0 & \frac{6EI}{h_3^2} & 0 & \frac{-6EI}{h_3^2} & 0 & 0 & 0 & 0 \\
0 & 0 & 0 & \frac{6EI}{h_3^2} & \frac{6EI}{d^2}-\frac{6EI}{h_3^2} & \frac{-6EI}{d^2} & 0 & 0 & 0 \\
0 & 0 & 0 & 0 & \frac{6EI}{d^2} & 0 & \frac{-6EI}{d^2} & 0 & 0 \\
0 & 0 & 0 & 0 & 0 & \frac{6EI}{d^2} & 0 & \frac{-6EI}{d^2} & 0 \\
0 & 0 & 0 & 0 & 0 & 0 & \frac{6EI}{d^2} & 0 & \frac{-6EI}{d^2} \\
0 & 0 & 0 & 0 & 0 & 0 & 0 & \frac{6EI}{d^2} & \frac{6EI}{d^2}
\end{bmatrix}$$

$$\mathbf{k}_{to} = \begin{bmatrix}
\frac{4EI}{h_1} & \frac{2EI}{h_1} & 0 & 0 & 0 & 0 & 0 & 0 & 0 \\
\frac{2EI}{h_1} & \frac{4EI}{h_1}+\frac{2EI}{h_2} & \frac{EI}{h_2} & 0 & 0 & 0 & 0 & 0 & 0 \\
0 & \frac{EI}{h_2} & \frac{2EI}{h_2}+\frac{4EI}{h_3} & \frac{2EI}{h_3} & 0 & 0 & 0 & 0 & 0 \\
0 & 0 & \frac{2EI}{h_3} & \frac{8EI}{h_3} & \frac{2EI}{h_3} & 0 & 0 & 0 & 0 \\
0 & 0 & 0 & \frac{2EI}{h_3} & \frac{4EI}{h_3}+\frac{4EI}{d} & \frac{2EI}{d} & 0 & 0 & 0 \\
0 & 0 & 0 & 0 & \frac{2EI}{d} & \frac{8EI}{d} & \frac{2EI}{d} & 0 & 0 \\
0 & 0 & 0 & 0 & 0 & \frac{2EI}{d} & \frac{8EI}{d} & \frac{2EI}{d} & 0 \\
0 & 0 & 0 & 0 & 0 & 0 & \frac{2EI}{d} & \frac{8EI}{d} & \frac{2EI}{d} \\
0 & 0 & 0 & 0 & 0 & 0 & 0 & \frac{2EI}{d} & \frac{4EI}{d}
\end{bmatrix}$$

Here the bending stiffness of the pile is the product of the modulus of elasticity (E) and the moment of inertia (I) of the pile. The spring constant of the fender is k_f and the soil spring constants are k_{S1} through k_{S5} as illustrated in Figure 5.2. The dimensions h_1, h_2, h_3, and d are also shown in Figure 5.2.

5.1.3 Damping

The energy losses that occur when a ship impacts a fender pile can be attributed to any combination of the following: viscous drag on the vessel and pile, generation of surface waves, and material losses within the pile, soil, rubber fenders, and vessel hull. The damping characteristics of a structure can typically be obtained by performing a free vibration test. In this test the structure is initially forced into a state of free vibration and the damping ratio is evaluated from the decay in the displacement, velocity, or acceleration amplitude over time. The damping ratio (ζ) can be approximated from the logarithmic decrement having the form (e.g. Chopra 2000)

$$\zeta = \frac{1}{2\pi N} \ln \frac{A_j}{A_{j+N}} \qquad \text{(Eq. 5.17)}$$

Where N is the number of cycles between two peak amplitude values A_j and A_{j+N}. In a fender pile system the vessel only remains coupled to the pile for ½-cycle. Therefore, the damping ratio can be estimated from the initial vessel velocity (V_{vo}) and the velocity when the vessel becomes decoupled from the pile (V_{fo}) using the following equation

$$\zeta_n = \zeta = \frac{1}{\pi} \ln \frac{V_{vo}}{\left|V_{vf}\right|} \qquad \text{(Eq. 5.18)}$$

For simplicity, a single damping ratio is used to characterize damping for all modes and degrees of freedom for the fender pile system. Damping for most civil structural systems is typically less than 20% (Chopra 2000).

5.2 Comparison of Model and Field Impact Test Results

This section presents again the results of the field impact tests performed on a fiber reinforced concrete (FRP) composite fender pile. This data was used to validate the new dynamic analysis approach.

5.2.1 Test Configuration and Results

A typical time history of velocity and displacement measured at the vessel impact location (ACC 2) is shown in Figure 5.3. As shown in the figure, the velocity increases rapidly from zero to 0.13 m/s within the first 0.2 seconds of impact. The velocity decreases more gradually to zero at the point of maximum pile displacement and then accelerates to a velocity of -0.07 m/s where the vessel becomes decoupled from the pile. The time between the points of maximum velocity is approximately 1.2 seconds. The maximum displacements calculated from the accelerometer data are summarized in Table 5.1. As shown in Table 5.1, the displacements obtained through integration of ACC 1 were typically within 6% of the displacements measured with the range finder.

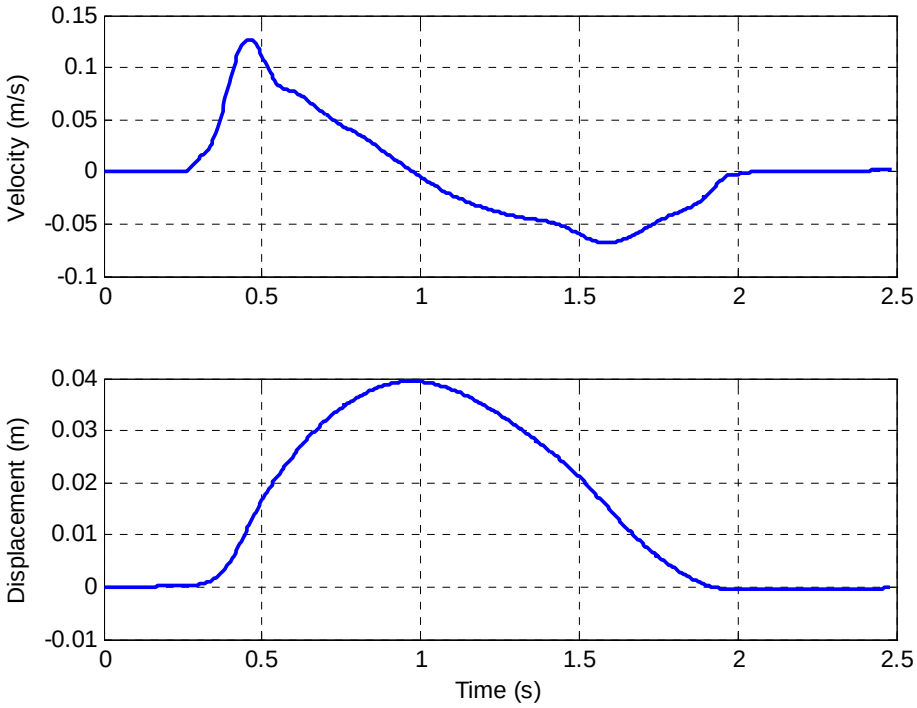

Figure 5.3. Typical velocity and displacement time history (Test 3) as integrated from the accelerometer mounted at the vessel impact point.

The accelerometer that was mounted near the impact point was also used to estimate the velocity of the vessel during impact. The mass of the vessel is significantly larger than the pile mass and therefore changes in the vessel's momentum at initial impact are anticipated to be negligible. As shown by the velocity time history shown in Figure 5.3 there are two points at which the velocity is a maximum; one just after the point of impact representing the initial velocity of the vessel and the second when the vessel becomes de-coupled with the pile. A summary of the initial and final vessel velocities from the tests are summarized in Table 5.2.

Table 5.1. Summary of maximum lateral pile displacements (in cm) recorded during the impact tests.

Test	Sonic Range Finder	ACC 1	ACC 2	ACC 3
1	3.78	3.93	2.74	1.80
2	4.42	4.69	3.66	2.96
3	4.66	4.94	3.93	3.35
4	5.24	5.09	5.43	5.18
5	4.42	4.51	3.90	2.62
6	4.36	4.48	3.60	2.13
7	4.66	4.05	3.60	2.80
8	4.79	4.91	3.87	2.74
Average	4.54	4.58	3.84	2.95

Table 5.2. Summary of velocities measured at the vessel impact point (ACC 2). The damping ratio was calculated from the velocities using Equation (5-18).

Test	Initial Velocity (m/s)	Final Velocity (m/s)	Damping Ratio
1	0.075	-0.042	0.18
2	0.112	-0.060	0.19
3	0.127	-0.068	0.19
4	0.169	-0.090	0.20
5	0.113	-0.064	0.18
6	0.106	-0.056	0.20
7	0.118	-0.063	0.20
8	0.124	-0.069	0.18
Average	0.118	-0.064	0.19

5.2.2 Mass Parameters

The mass of the pile itself was distributed among the lumped masses based on the spacing between nodes. The manufacturers stated pile unit weight of 22.9 kN/m^3 was used in the analysis. In addition to pile mass, mass m_2 also included the vessel mass and hydrodynamic added mass. The virtual mass (m_v), or the sum of the vessel mass and hydrodynamic added mass was estimated from a virtual mass coefficient (C_m) where

$$m_v = C_m m_{vessel} \qquad \text{(Eq. 5.19)}$$

A C_m value of 1.1 was used because it is applicable to a vessel moving head-on (Gaythwaite 2004). In addition to pile mass, masses m_3 and m_4 included hydrodynamic added mass of the pile moving transversely through the water. The added mass the pile under this condition was taken to be the mass of water displaced by the pile itself (Newman 1978).

5.2.3 Stiffness Parameters

The bending stiffness of the fender pile was determined from 4-point bending test data performed on the same pile type (Rutgers 1996). The test results, which are shown in Figure 5.4, were used to calculate the pile stiffness (EI) using the following equation (Lampo et al. 1998)

$$EI = \frac{Pa}{48\delta}\left(3L^2 - 4a^2\right) \qquad \text{(Eq. 5.20)}$$

In the load test a was 1.016 m and L was 3.048 m. As shown in Figure 5.4 the stress-strain curve is slightly non-linear. Since the model requires a linear stiffness, a tangent modulus of 2.66 x 10^6 N-m^2 was calculated at 20% of the ultimate moment. This criteria is consistent with other composite pile manufacturer's guidelines (e.g. Hardcore Composites).

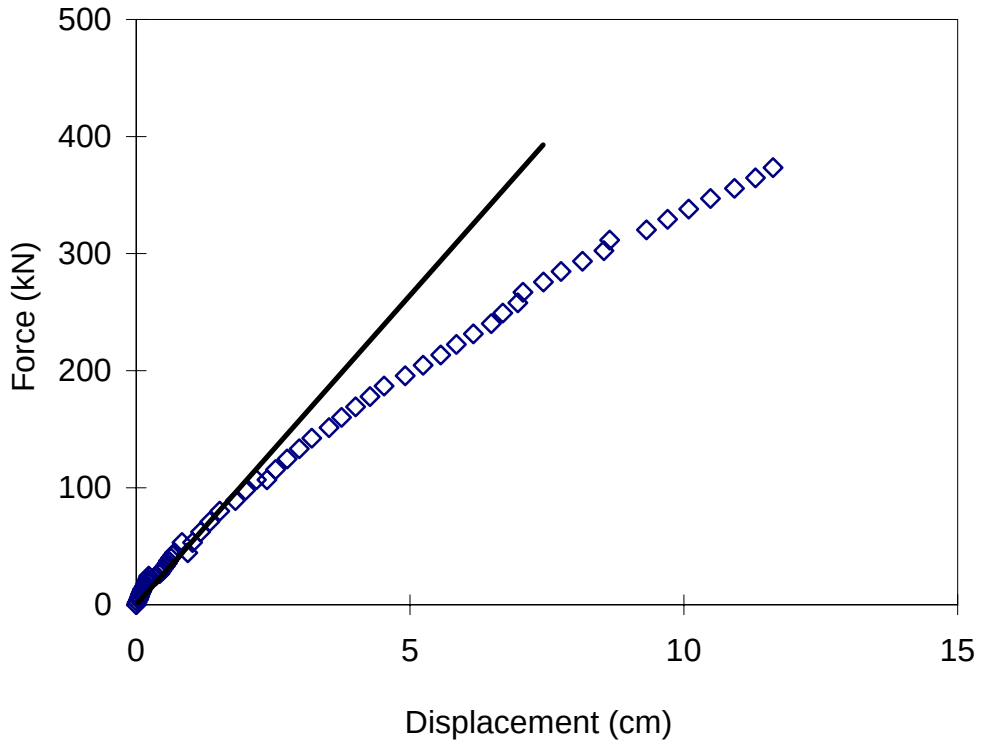

Figure 5.4. Results of 4-Point bending test performed on a 12.75-inch diameter Landcaster CP 40 pile (after Rutgers 1996). The tangent modulus evaluated at 20% of the failure load is shown by the line.

The test pile was laterally supported at deck level by a rubber V-shaped fender. The spring constant for the fender element was evaluated from a laboratory compression test. The stiffness parameters used in the model represent the static stiffness of the system and thus the load test was performed slow enough (≈1 cm/min) so as not to include dynamic effects. A section of fender was placed in a load frame and a constant rate of strain was applied while measuring the load. Reactions were applied through a 12.75-inch diameter circular wood block to simulate the contact geometry between the fender and pile. A spring constant (k_f) of 190,900 N/m was determined from the test data shown in Figure 5.5.

The soil stiffness was estimated using published values of the modulus of lateral subgrade reaction (K_h). Core samples taken nearby indicate that the upper soils consist of interbedded silts and sands. Values of K_h for this soil type are in the range of 100 to 200 MN/m^3 (Bowles 1988). The soil spring constants were assumed to be constant with depth and were determined from the pile diameter (w) and spacing between nodes below the mudline (d).

$$k_{si} = K_h \cdot d \cdot w \qquad \text{(Eq. 5.21)}$$

The spring constant of the node at the mudline was reduced by 50% since the effective depth of soil influencing this node is $d/2$.

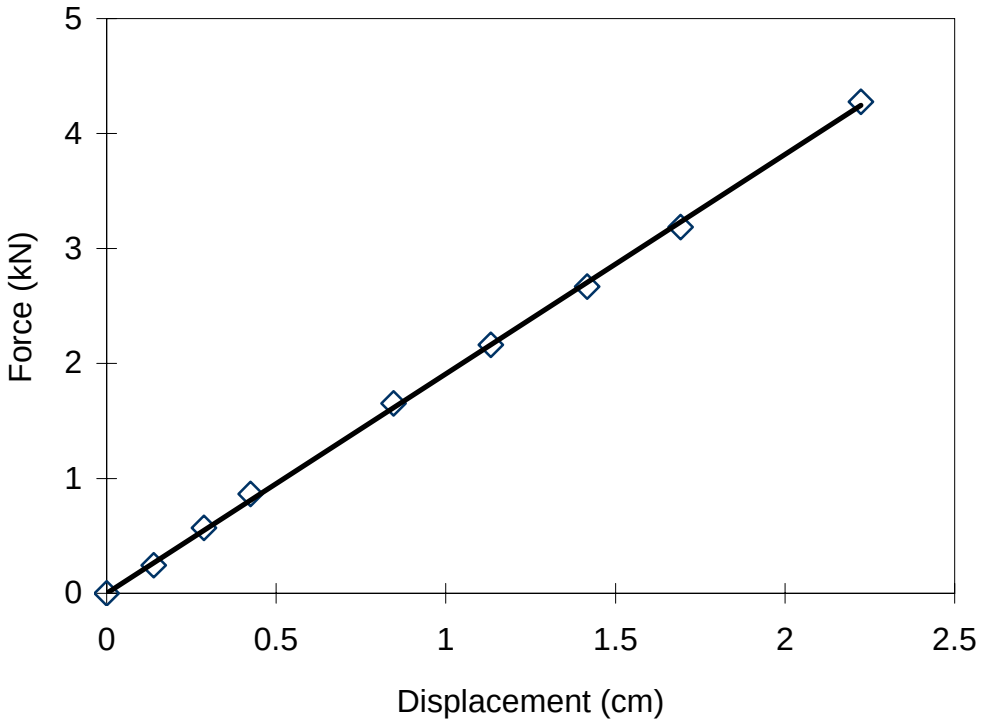

Figure 5.5. Results of the static compression test performed on a section of rubber fender.

5.2.4 Damping Parameters

Using Equation (5.18) and the vessel velocity data from Table 5.2 the damping ratio was calculated for each test. These values, which are also shown in Table 5.2, range from 18 to 21% with an average value of 19%. The calculated damping values appear to be reasonable considering that they are within the upper range of published values.

5.2.5 Comparison of Field Test and Model Data

Model calculations were made for comparison to the measured field data using the parameters given above. Figure 5.6 shows typical modeled displacement and velocity time histories at the impact point using an average velocity of 0.12 m/s and a damping of 19%. The time between the peak velocities for the model was determined to be about 1.1 seconds which compares favorably with the measured time of 1.2 seconds (Figure 5.3). Since the damped natural frequency is controlled primarily by the stiffness and mass, the close agreement between the modeled and measured results suggests that these parameters are reasonable.

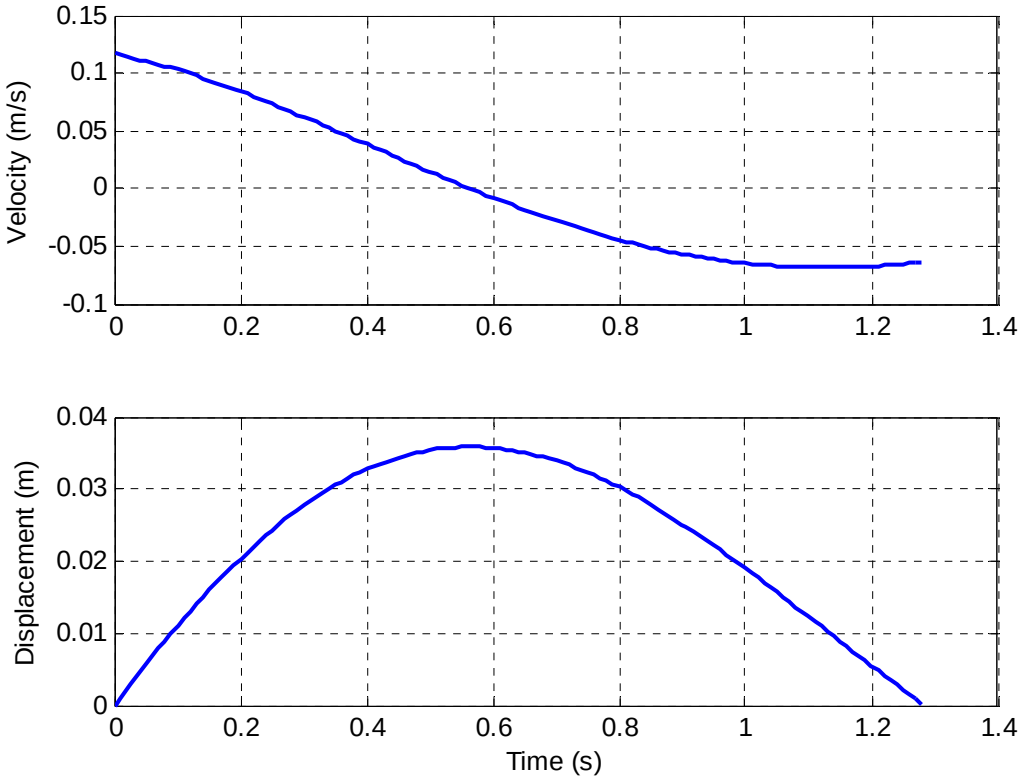

Figure 5.6. Modeled displacement at the impact point using an average vessel velocity of 0.12 m/s and 19% damping.

The maximum lateral displacements measured along the length of the pile as averaged from all impact tests (Table 5.1) are plotted in Figure 5.7. The maximum displacements calculated with the dynamic model for an average velocity of 0.12 m/sec and a damping of 19% are also shown in the figure. For comparison, the kinetic energy method was used to calculate maximum displacements using the same stiffness matrix used in the dynamic model. The kinetic energy method is included in the comparison because it represents a condition having zero energy losses (i.e. no damping).

Given the selected parameters, the displacements calculated in both the dynamic and static models compare reasonably well with the field data. The kinetic energy method, however, yielded slightly higher displacements relative to both the modeled and the measured values. Most importantly, by incorporating damping into the system the maximum displacement at the impact point is reduced by about 25 percent. For a linear system this is equivalent to a 25 percent reduction in the forces and moments on the pile. From a design perspective, lower stresses may justify the use of smaller piles (or fewer piles) resulting in cost savings.

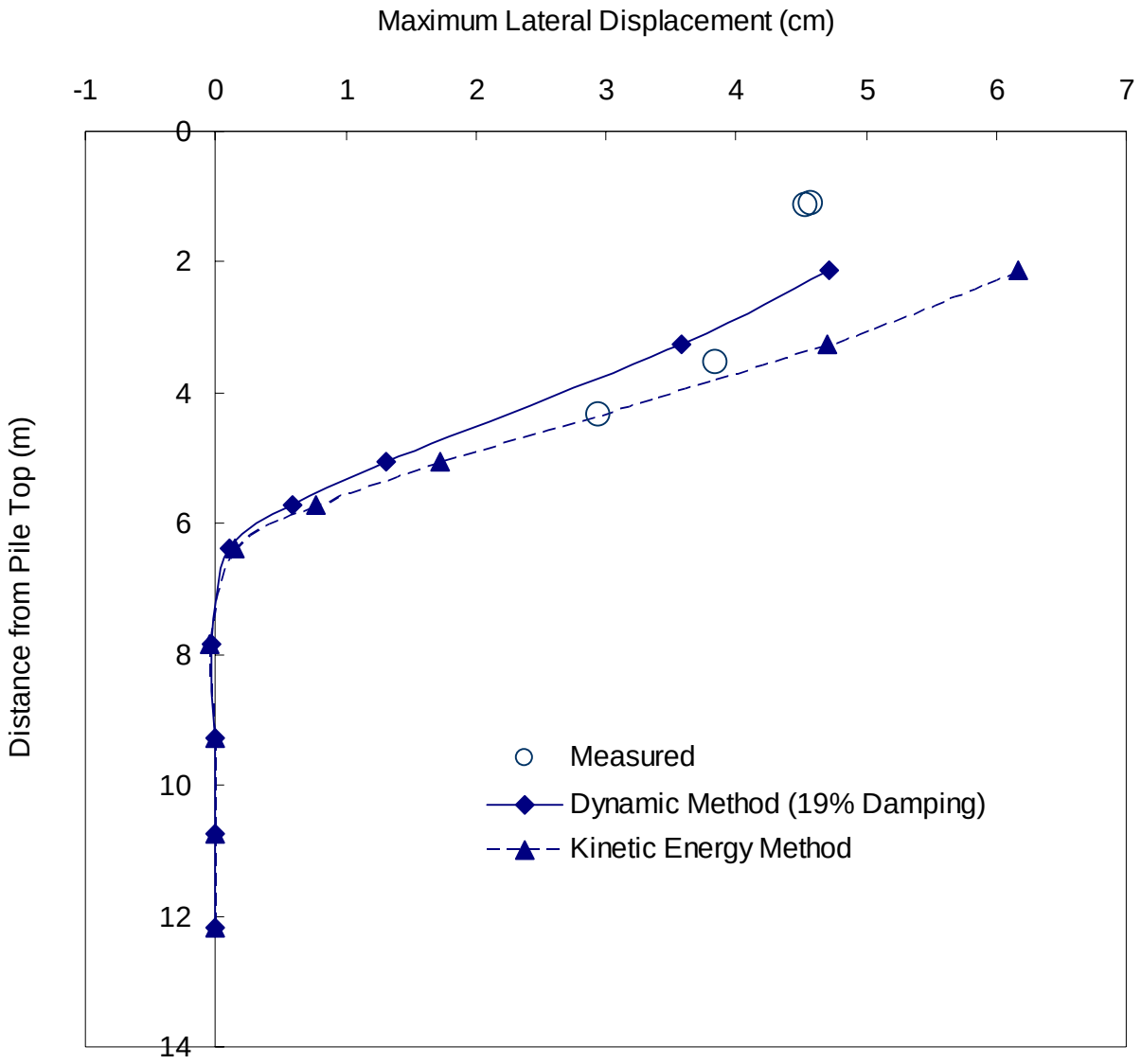

Figure 5.7. Comparison of modeled and average measured displacements along the length of the pile for an average vessel velocity of 0.12 m/s.

6.0 Conclusions

The primary objectives of this research study were to improve the understanding of the performance of composite piles as a fendering system in the marine environment. Specific areas of study included an evaluation of driving stresses during hard driving conditions (i.e. bedrock) and the response of composite piles to lateral impact loads.

This was accomplished through two separate field studies in which concrete-filled FRP pipe piles and steel reinforced plastic piles were installed at a residential site in Old Greenwich, CT and along a pier at Fort Wetherill in Jamestown, RI. The piles in Old Greenwich were driven to failure with a hydraulic hammer and PDA and CAPWAP analyses were performed. It was found that the Pile Integrity Tester (PIT) was effective in measuring damage of the FRP pile due to driving. It was difficult to obtain PIT results with the plastic pile. Definitive conclusions regarding CAPWAP and driving stresses could not be made because of problems installing the piles to sufficient depths. It was particularly difficult to anchor accelerometers and strain gauges in the FRP pile.

The piles at Fort Wetherill were impacted with an 85 ton vessel at low speeds and the dynamic response of the piles was measured using accelerometers and displacement transducers. The acceleration time histories were integrated twice to obtain the displacements using the program MATLAB. The results indicated that the piles absorbed the impact energy through both translation and bending, and the overall stiffness of the fender system was estimated using the kinetic energy approach.

A new dynamic analysis approach was developed for the design of these flexible fender piles. Unlike the traditional kinetic energy method, the dynamic approach considers the energy losses in the system (i.e. damping) that occurs during vessel impact. Damping in a fender system is a useful parameter for quantifying its energy dissipation characteristics. The model accounts for the stiffness contributions of all fender components including rubber fender supports, pile, and soil. Impact test results performed on an FRP composite pile were used to evaluate the damping properties of this fender pile system, and to validate the dynamic model. An average damping of 19% was estimated using the velocity time history of the vessel recorded during impact. Incorporating this value of damping the displacements obtained from the dynamic model compare well with the measured data in terms of the impact duration and maximum displacements. As compared to the kinetic energy approach, the dynamic approach reduced the displacements, forces, and moments by about 25 percent. Additional studies of the damping characteristics of other pile types such as timber and plastic piles may provide further insight on the relative design benefits of using these pile types for fendering applications.

7.0 Acknowledgements

This study was made possible by a grant from the University of Rhode Island Transportation Center and in-kind support from the following organizations: G. Donaldson Construction Co., Inc., GZA Geoenvironmental, Inc., Heller and Johnsen, Lancaster Composite, Plastic Pilings, Inc., and the Rhode Island Department of Environmental Management. Their assistance is greatly appreciated. Special thanks to Francois Enet, Jason Ressler, and Fred Pease for help with the instrumentation and field impact tests. The authors would also like to acknowledge the insightful comments of the anonymous reviewer in the development of the new analysis and design method presented in Chapter 5.

8.0 References

Bowles, J. E. (1988). *Foundation Analysis and Design*, McGraw-Hill Publishing Company, New York.

Chopra, A.K. (2000). *Dynamics of Structures: Theory and Applications to Earthquake Engineering*, Prentice Hall, New Jersey.

Fellenius, B. H., Riker, R. E., O'Brien, A. J., and Tracy, G. R. (1989). "Dynamic and Static Testing in Soils Exhibiting Setup." American Society of Civil Engineers, *Journal of Geotechnical Engineering*, 115(7), pp. 984-1001.

FHWA (1998). "Design and Construction of Driven Pile Foundations, Vol. II," U.S. Department of Transportation Federal Highway Administration, National Highway Institute, Publication No. FHWA HI 97-014.

Gaythwaite, J.W. (2004). *Design of Marine Facilities*, ASCE Press, Reston, Virginia.

Goble, Rausch, Likins, and Associates, Inc. (2000). "PDA Results - Pipe Extension No.4 Beach Erosion Control Project", Hardcore Composite Report, Report No.2000HCR0030.

Gummert, M. N. (2003). Evaluation of the Drivability of Composite Piles. Master's Thesis, University of Rhode Island, 220p.

Iskander, M.G. and Hassan, M. (1998). "State of the Practice Review in FRP Composite Piling," *Journal of Composites for Construction*, August, pp. 116-120.

Iskander, M.G. and Stachula, A. (1999). "FRP Composite Polymer Piling: An Alternative to Timer Pilling for Water-Front Applications," *Geotechnical News*, pp. 27-29.

Iskander, M.G., Hanna, S., and Stachula, A. (2001). "Drivability of FRP Composite Piling," *Journal of Geotechnical and Geoenvironmental Engineering*, February, pp.169-176.

Iskander, M.G., and Stachula, A. (2001). "Drivability of FRP Composite Piling," *Journal of Geotechnical and Geoenvironmental Engineering*, 127(2), pp.169- 176.

Iskander, M.G., and Stachula, A. (2002).

Kinsler, L. E., Frey, A. R., Coppens, A. B., and Sanders, J. V. (1982). Fundamentals of Acoustics, 3RD Edition. Canada, John Wiley & Sons, Inc.

Kistler Instrument Corporation (2004). Website: www.kistler.com.

Kozera, D.W. (1996) Dynamic Pile Testing, Hardcore Composites Report, Report No. 2000HCR0004.

Lampo, R., Nosker, T., Barno, D. Busel, J., Maher, A., Dutta, P., and Odello, R. (1998). "Development and Demonstration of FRP Composite Fender, Loadbearing, and Sheet Piling Systems," *USACERL Technical Report 98/123*, September.

Leet, K.M. (1988). *Fundamentals of Structural Analysis*. Macmillan Publishing Company, New York.

Li, S., Ramakrishnan, V. (1971). "Ultimate energy design of prestressed concrete fender piling." *J. Waterways, Harbors, and Coastal Engineering Division, ASCE*, 97(WW4), 647-662.

Maher, M.H., Gucunski, N., and Chae, Y. S. (1996). "Composite Fender and Sheet Piles in Marine Front Systems," *Proceedings of First International Conference on Composites in Infrastructure*, ICCI' 96, Tucson, AZ.

Massa Products Corporation (1998). Website: www.massa.com

Newman, J.N. (1977). *Marine Hydrodynamics*, MIT Press, Cambridge, Massachusetts.

Pando, M. A., Filz, G. M., Early, C., Hoppe, E. (2003). "Axial and Lateral Load Performance of Two Composite Piles and One Prestressed Concrete Pile." TRB 2003 Annual Meeting CD-ROM, Paper No: 03-2912.

Pando, M. A., Brown, D., and Filz, G. M. (2004). "Performance of Laterally Loaded Composite Pile at the Nottoway River Bridge," GeoTrans Conference Proceedings, Geotechnical Engineering for Transportation Projects, ASCE GSP No. 126.

Pile Dynamics, Inc. (2002). "GRLWEAP Wave Equation Analysis of Pile Driving Procedures and Models Version 2002".

Rausche, F., Likins, G. E., Goble, G. G., and Miner, R. (1985). "The Performance of Pile Driving Systems." Main Report, U.S. Department of Transportation, Federal Highway Administration, Office of Research and Development, Washington, D.C.

Reese, L.C., O'Neill, M.W., and Radhakrishnan, N. (1970). "Rational design concept for breasting dolphins." *J. Waterways and Harbors Division, ASCE*, 96(WW2), 433-450.

Rizkalla, S.H., Fam, A.Z. (1999). State-of-the-art Report on Stay- In-Place FRP Formwork, submitted to ACI Committee 440 J, Lancaster Composite, Inc. Technical Reference Part 1.

Rutgers (1996). "Flexure tests of 12.75" diameter Composite Post 40 piles-preliminary report." Department of Civil and Environmental Engineering, Rutgers University.

USACE (1983). *Engineering and Design of Military Ports*. TM 5-850-1, US Army Corps of Engineers.

APPENDIX A:

MATLAB code used to filter, integrate, and plot the data from the field impact tests.

```
% This program was written by Jason Ressler on August 24, 2004.
% For use by URI Marine Geomechanics Lab Composite Piles project, funded by DOT
% For use by Chris Baxter, Arron Bradshaw, and Anthony Marinucci.
%
% This program will :
% 1) Load accelerometer and range finder data taken at Fort Weatherill.
% 2) Prove validity of accelerometer data by integrating it twice to find displacement and subsequent
%    comparison with displacement pile data from the sonic range finder.  Accelerometer 1 (A1) and range
finder
%    (D1) were mounted within 1 ft of each other and should read similar.
% 3) Filter accelerometer and sonic range finder data (before and/or after integration) to eliminate
%    system noise.
% 4) After accelerometer data is validated, the same filters and integration techniques will be
%    applied to the other three accelerometers to find a log of displacement over time for the
%    length of the pile.
%
% A total of 15 tests were done.  6 on a plastic pile and 9 on a fiber reinforced pile.  Analysis will be
% done for each test.

clear all
close all
clc

%       PHYSICAL CONSTANTS
g           =       32.2;                                   %       Earth's Gravitational Acceleration
        (ft/s^2)
Tpi         =       2*pi;                                   %       Two times pi
                            (d'less)

%       EXPERIMENTAL FACTORS
fs                  =       200.00;                         %       Sampling frequency (Scan
Rate)               (Hz)

%       CONVERSION FACTORS

%       CALIBRATION FACTORS
m1                  =       0.9989;                         %       accelerometer 1
calibration         (g/volts)
b1                  =       0.017;                          %       accelerometer 1 y-
intercept(g)
m2                  =       0.9893;                         %       accelerometer 2
calibration         (g/volts)
b2                  =       0.0514;                         %       accelerometer 2 y-
intercept(g)
m3                  =       4.9396;                         %       accelerometer 3
calibration         (g/volts)
b3                  =       -0.0596;                %       accelerometer 3 y-intercept
        (g)
m4                  =       4.9775;                         %       accelerometer 4
calibration         (g/volts)
b4                  =       -0.0203;                %       accelerometer 4 y-intercept
        (g)
m5                  =       16.787;                     %       sonic range finder calibration
(inch/volts)
b5                  =       -5.1742;                %       sonic range finder 1 y-intercept
(inch)
```

```
% Determine the number of files we would like to analyze
filenames = dir('*.txt');

% Load each file, one at a time, and perform analysis.
for i = 1:length(filenames);
   filenames(i).name
   temp = load(filenames(i).name);
   Acc_Volts_1=temp(:,1);
   Acc_Volts_2=temp(:,2);
   Acc_Volts_3=temp(:,3);
   Acc_Volts_4=temp(:,4);
   Range_Volts=temp(:,5);

   % Calibrate voltage data to acceleration and displacement data
   Acc_Data_1=g*m1.*Acc_Volts_1 + b1;%          accelerometer 1 vector          (ft/s^2)
   Acc_Data_2=g*m2.*Acc_Volts_2 + b2;%          accelerometer 2 vector          (ft/s^2)
   Acc_Data_3=g*m3.*Acc_Volts_3 + b3;%          accelerometer 3 vector          (ft/s^2)
   Acc_Data_4=g*m4.*Acc_Volts_4 + b4;%          accelerometer 4 vector          (ft/s^2)
   Range_Data=m5.*Range_Volts + b5;%    range finder vector                     (inch)
   Range_Data=Range_Data./12;%        covert to feet


   % Isolating the signal section of interest.
   % Determine when the impact occurs.
   % Accelerometer 2 was closest to the impact zone.
   % We will assume that it responds first and use it to find a cutoff time
   startmax=ceil(0.1*length(Acc_Data_1));
   endmax=floor(0.2*length(Acc_Data_1));

   Max_Acc_2_static=max(Acc_Data_2(startmax:endmax));
   cutofftimeindeces=find(Acc_Data_2>ceil(Max_Acc_2_static+1));
   cutofftimeindex=cutofftimeindeces(1);
   backofftimeindex=250; % Number of time steps before the signal start to include.
   starttimeindex=cutofftimeindex-backofftimeindex;
   signallengthindex=800;
   endtimeindex=starttimeindex+signallengthindex;

   Acc_Data_1a=Acc_Data_1(starttimeindex:endtimeindex);
   Acc_Data_2a=Acc_Data_2(starttimeindex:endtimeindex);
   Acc_Data_3a=Acc_Data_3(starttimeindex:endtimeindex);
   Acc_Data_4a=Acc_Data_4(starttimeindex:endtimeindex);
   Range_Dataa=Range_Data(starttimeindex:endtimeindex);

   % Find the mean signal of each data set before impact.  This will be
   % used to adjust the curve around zero
   % The zero adjustment will be found by averaging the data from 10 to 30
   % percent and 90 to 100 percent of the signal.  The signal must not
   % fall within these areas, only noise.

   startone=ceil(0.1*length(Acc_Data_1));
   endone=floor(0.3*length(Acc_Data_1));
   starttwo=ceil(0.9*length(Acc_Data_1));
   endtwo=floor(1.0*length(Acc_Data_1));
```

```
mm=mean(Acc_Data_1(startone:endone));
mmm=mean(Acc_Data_1(starttwo:endtwo));
m=[mm mmm];
Mean_Acc_1=mean(m);

mm=mean(Acc_Data_2(startone:endone));
mmm=mean(Acc_Data_2(starttwo:endtwo));
m=[mm mmm];
Mean_Acc_2=mean(m);

mm=mean(Acc_Data_3(startone:endone));
mmm=mean(Acc_Data_3(starttwo:endtwo));
m=[mm mmm];
Mean_Acc_3=mean(m);

mm=mean(Acc_Data_4(startone:endone));
mmm=mean(Acc_Data_4(starttwo:endtwo));
m=[mm mmm];
Mean_Acc_4=mean(m);


% Find shift offsett or mean of range data excluding the peaks caused
% by instrument noise
d=1;
for p=startone:1:endone;
   if  abs(Range_Data(p)-Range_Data(p+1)) <= 0.01
      Mean_Range_Data(d)=Range_Data(p);
      d=d+1;
   end
end
Mean_Range=mean(Mean_Range_Data);

% Subtract mean offsets to shift curves and data around zero
Acc_Data_1b=Acc_Data_1a-Mean_Acc_1;
Acc_Data_2b=Acc_Data_2a-Mean_Acc_2;
Acc_Data_3b=Acc_Data_3a-Mean_Acc_3;
Acc_Data_4b=Acc_Data_4a-Mean_Acc_4;
Range_Datab=Range_Dataa-Mean_Range;

% Create a time vector for the data based on the step size
timesteps=length(Acc_Data_1b);
time=[0:1/fs:(timesteps-1)/fs];
timeacc=[0:1/fs:(timesteps-1)/fs];
timevel=[0:1/fs:(timesteps-2)/fs];
timedisp=[0:1/fs:(timesteps-3)/fs];

% Plot the four accelerometer data and the range finder data
%    figure
%    subplot(5,1,1);plot(time,Acc_Data_1b);
%    ylabel('ft/sec^2');
%    set(gca,'xticklabel',[])
%    title(filenames(i).name);
%    legend('Acc 1 Not Filtered');
%    axis([0 4 -10 10]);
%
```

```
%     subplot(5,1,2);plot(time,Acc_Data_2b);
%     ylabel('ft/sec^2');
%     set(gca,'xticklabel',[]);legend('Acc 2 Not Filtered');
%     axis([0 4 -10 10]);
%
%     subplot(5,1,3);plot(time,Acc_Data_3b);
%     ylabel('ft/sec^2');
%     set(gca,'xticklabel',[]);legend('Acc 3 Not Filtered');
%     axis([0 4 -10 10]);
%
%     subplot(5,1,4);plot(time,Acc_Data_4b);
%     ylabel('ft/sec^2');
%     set(gca,'xticklabel',[]);legend('Acc 4 Not Filtered');
%     axis([0 4 -10 10]);
%
%     subplot(5,1,5);plot(time,Range_Datab);
%     ylabel('ft');
%     xlabel('Time (sec)');legend('Disp Not Filtered');
%     axis([0 4 -0.2 0.2]);


   % Define the data matrix (this is shifted around zero and cropped for
   % the impact zone.
   accdata=[Acc_Data_1b Acc_Data_2b Acc_Data_3b Acc_Data_4b];

   % Filter data.  This must be done before the integrations so that the
   % noise is not integrated and therefore compunded throughout the
   % cumulative integration
   order=1;       % this is the order of the butterworth filter
   cutoff=0.05;    % cutoff frequency (nondimensionnal see help)
   [B,A] = butter(order,cutoff);
   if i==4;
      figure;
      subplot(4,2,2);plot(time,accdata(:,1));
      axis([0 4 -10 10]);text(2,-8,'Acc 1 Unfiltered');
      set(gca,'xticklabel',[]);
      ylabel('ft/sec^2');

      subplot(4,2,4);plot(time,accdata(:,2));
      axis([0 4 -10 10]);text(2,-8,'Acc 2 Unfiltered');
      set(gca,'xticklabel',[]);
      ylabel('ft/sec^2');

      subplot(4,2,6);plot(time,-1.*accdata(:,3));
      axis([0 4 -10 10]);text(2,-8,'Acc 3 Unfiltered');
      set(gca,'xticklabel',[]);
      ylabel('ft/sec^2');

      subplot(4,2,8);plot(time,-1.*accdata(:,4));
      axis([0 4 -10 10]);text(2,-8,'Acc 4 Unfiltered');
      xlabel('sec');
      ylabel('ft/sec^2');

   end
   plc=1;
   for m=1:1:4;
```

```
   accfilt(:,m) = filter(B,A,accdata(:,m));

   if i==4;
      subplot(4,2,plc);
      if plc == 5;
         plot(time,-1.*accfilt(:,m));
      elseif plc == 7;
         plot(time,-1.*accfilt(:,m));
      else
         plot(time,accfilt(:,m));
      end
      ylabel('ft/sec^2');
      axis([0 4 -10 10]);

      if m==1; text(2,-8,'Acc 1 Filtered');set(gca,'xticklabel',[]);
         text(3,14,'Fiber Reinforced Pile Test 4');
      elseif m==2; text(2,-8,'Acc 2 Filtered');set(gca,'xticklabel',[]);
      elseif m==3; text(2,-8,'Acc 3 Filtered');set(gca,'xticklabel',[]);
      elseif m==4; text(2,-8,'Acc 4 Filtered');xlabel('sec');
      end
      plc=plc+2;
   end

end

% Now that all of the data is corrected and filtered, plot this on a
% subplot includign acceleration from acc 1 - 4 and disp from sonic

figure

subplot(5,1,1);plot(time,accfilt(:,1));
ylabel('ft/sec^2');
set(gca,'xticklabel',[])
title(filenames(i).name);
text(2.5,7,'Accelerometer 1 Filtered');
axis([0 4 -10 10]);

subplot(5,1,2);plot(time,accfilt(:,2));
ylabel('ft/sec^2');
set(gca,'xticklabel',[]);text(2.5,7,'Accelerometer 2 Filtered');
axis([0 4 -10 10]);

subplot(5,1,3);plot(time,-1.*accfilt(:,3));
ylabel('ft/sec^2');
set(gca,'xticklabel',[]);text(2.5,7,'Accelerometer 3 Filtered');
axis([0 4 -10 10]);

subplot(5,1,4);plot(time,-1.*accfilt(:,4));
ylabel('ft/sec^2');
set(gca,'xticklabel',[]);text(2.5,7,'Accelerometer 4 Filtered');
axis([0 4 -10 10]);

subplot(5,1,5);plot(time,Range_Datab);
ylabel('ft');
xlabel('Time (sec)');text(2.5,0.13,'Sonic Range Finder');
axis([0 4 -0.2 0.2]);
```

```
% Integrate the accelerometer data twice to determine the displacement
% Note that each data point is integrated from 0 to t where t is the
% time of the data point of interest during each loop.  Integrations
% are cumulative and are NOT the area of a single slice of width dt.

% Integration 1
for j=1:1:4;
   vnot=0;
   for k=1:1:length(accfilt(:,1))-1;
      accdataint1(k,j)=(1/(2*fs)).*(accfilt(k+1,j)+accfilt(k,j))+vnot;
      vnot=accdataint1(k,j);
   end
end
% Integration 2
for j=1:1:4;
   xnot=0;
   for k=1:1:length(accdataint1(:,1))-1;
      accdataint2(k,j)=(1/(2*fs)).*(accdataint1(k+1,j)+accdataint1(k,j))+xnot;
      xnot=accdataint2(k,j);
   end

   % Plot the Accelerometer data in subplots as acceleration,
   % velocity, and displacement.  Each accelerometer and integrations
   % are plotted on separate figures.
   if i==4 & j==1;
      figure
      subplot(3,1,1);plot(timeacc',accfilt(:,j));axis([0 4 -10 10]);
      text(0.25,7,'Acceleration');
      set(gca,'xticklabel',[]);
      title('Fiber Reinforced Pile Test 4');
      ylabel('ft/sec^2');
%
%        if j==1; text(3,10,'Accelerometer 1');
%        elseif j==2; text(3,10,'Accelerometer 2');
%        elseif j==3; text(3,10,'Accelerometer 3');
%        elseif j==4; text(3,10,'Accelerometer 4');
%        end

      subplot(3,1,2);plot(timevel',accdataint1(:,j));axis([0 4 -1 1]);
      text(0.25,0.5,'Velocity');
      set(gca,'xticklabel',[]);ylabel('ft/sec');

      subplot(3,1,3);plot(timedisp',accdataint2(:,j),time,Range_Datab);axis([0 4 -0.3 0.3]);
      text(0.25,0.2,'Displacement');
      legend('Acceleration Derived','Sonic Range Finder');
      ylabel('ft');xlabel('sec');
   end

end
% Verify that the integrated accelerometer 2 data is similar to the
% range finder data

%    figure
%    plot(time,Range_Datab,timedisp,accdataint2(:,1));
```

```
%     title(filenames(i).name);
%     text(0.5,-0.18,'Range finder and Accelerometer Displacement Comparison');
%     xlabel('Time (sec)');
%     ylabel('Displacement (ft)');
%     legend('Range Finder','Integrated Accelerometer');

    % Plot all displacement data together
    figure

    subplot(4,1,1);
    plot(timedisp,accdataint2(:,1),time,Range_Datab);
    title(filenames(i).name);
    set(gca,'xticklabel',[]);ylabel('ft');
    text(0.25,0.2,'Range Finder and Integrated Accelerometer 1');
    axis([0 4 -0.3 0.3]);

    subplot(4,1,2);
    plot(timedisp,accdataint2(:,2));ylabel('ft');
    axis([0 4 -0.3 0.3]);set(gca,'xticklabel',[]);
    text(0.25,0.2,'Integrated Accelerometer 2');

    subplot(4,1,3);
    plot(timedisp,-1.*accdataint2(:,3));ylabel('ft');
    axis([0 4 -0.3 0.3]);set(gca,'xticklabel',[]);
    text(0.25,0.2,'Integrated Accelerometer 3');

    subplot(4,1,4);
    plot(timedisp,-1.*accdataint2(:,4));ylabel('ft');
    axis([0 4 -0.3 0.3]);
    text(0.25,0.2,'Integrated Accelerometer 4');
    xlabel('sec');


    % Now find the maximum displacement throughout the depth of the pile
    % This array will have columns that contain accelerometer data 1
    % through 4 integrated twice to find displacement in coulumn 1 through
    % 4 and the fifth column will be displacement found via the range
    % finder.  All acc data has been filtered.

    dispmax1=min(accdataint2(:,1));
    dispmax2=min(accdataint2(:,2));
    dispmax3=max(accdataint2(:,3));
    dispmax4=max(accdataint2(:,4));
    dispsonic=min(Range_Datab);


    master_displacement(i,:)=[dispmax1 dispmax2 dispmax3 dispmax4 dispsonic];

end
```

APPENDIX B:

Filtered acceleration and integrated displacement data for all tests on FRP and PPI piles.

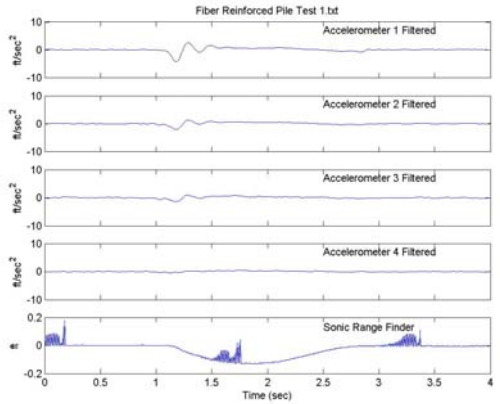
Fiber Reinforced Pile Test 1.txt
Accelerometer 1 Filtered
Accelerometer 2 Filtered
Accelerometer 3 Filtered
Accelerometer 4 Filtered
Sonic Range Finder
ft/sec²
ft
Time (sec)

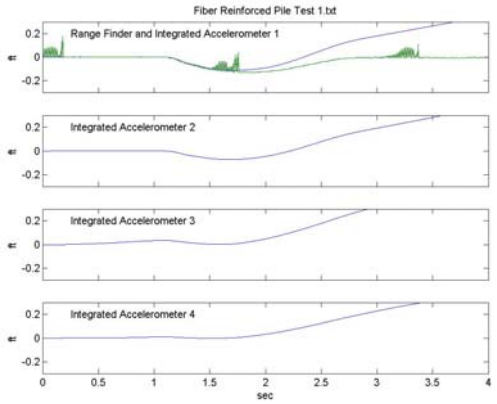
Fiber Reinforced Pile Test 1.txt
Range Finder and Integrated Accelerometer 1
Integrated Accelerometer 2
Integrated Accelerometer 3
Integrated Accelerometer 4
ft
sec

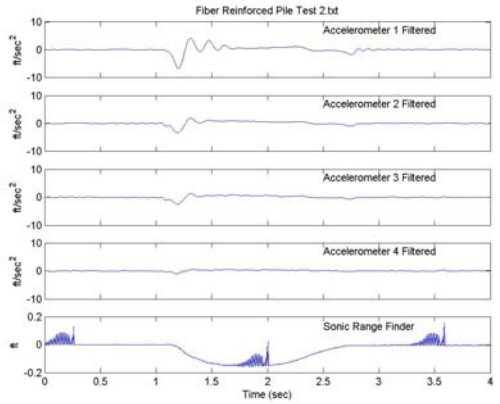
Fiber Reinforced Pile Test 2.txt
Accelerometer 1 Filtered
Accelerometer 2 Filtered
Accelerometer 3 Filtered
Accelerometer 4 Filtered
Sonic Range Finder
ft/sec²
ft
Time (sec)

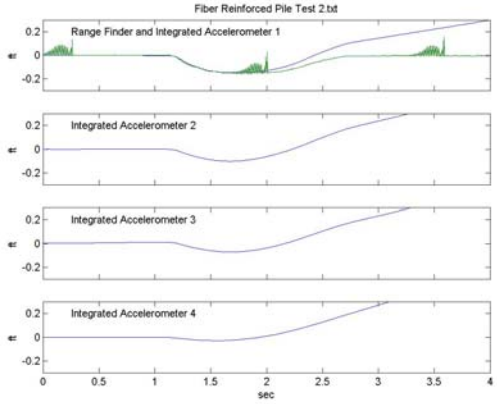
Fiber Reinforced Pile Test 2.txt
Range Finder and Integrated Accelerometer 1
Integrated Accelerometer 2
Integrated Accelerometer 3
Integrated Accelerometer 4
ft
sec

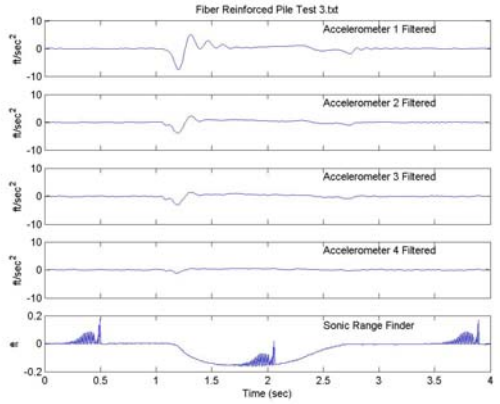
Fiber Reinforced Pile Test 3.txt
Accelerometer 1 Filtered
Accelerometer 2 Filtered
Accelerometer 3 Filtered
Accelerometer 4 Filtered
Sonic Range Finder
ft/sec²
ft
Time (sec)

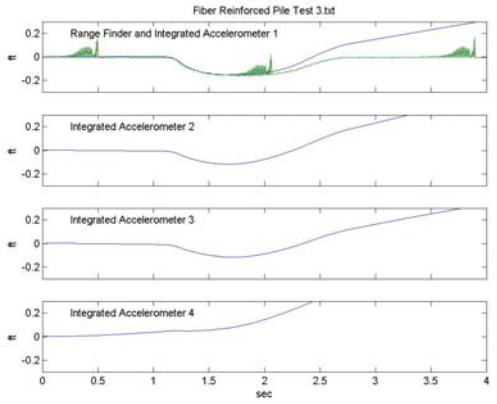
Fiber Reinforced Pile Test 3.txt
Range Finder and Integrated Accelerometer 1
Integrated Accelerometer 2
Integrated Accelerometer 3
Integrated Accelerometer 4
ft
sec

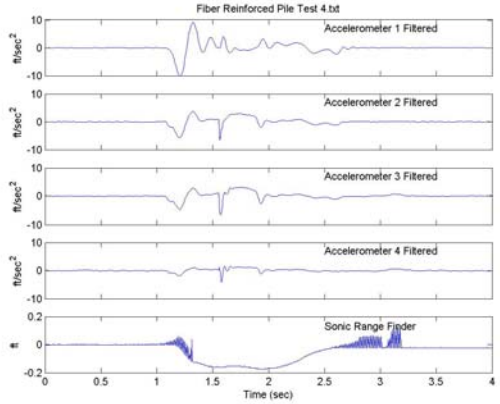
Fiber Reinforced Pile Test 4.txt
Accelerometer 1 Filtered
Accelerometer 2 Filtered
Accelerometer 3 Filtered
Accelerometer 4 Filtered
Sonic Range Finder
ft/sec²
ft
Time (sec)

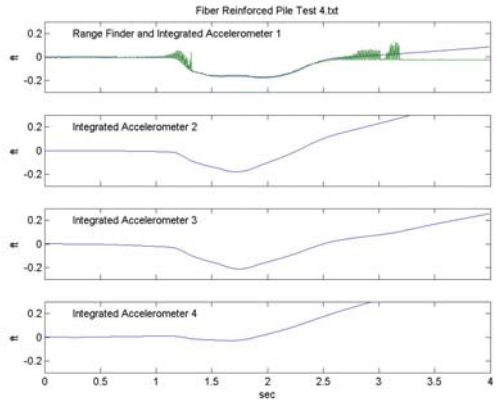
Fiber Reinforced Pile Test 4.txt
Range Finder and Integrated Accelerometer 1
Integrated Accelerometer 2
Integrated Accelerometer 3
Integrated Accelerometer 4
ft
sec

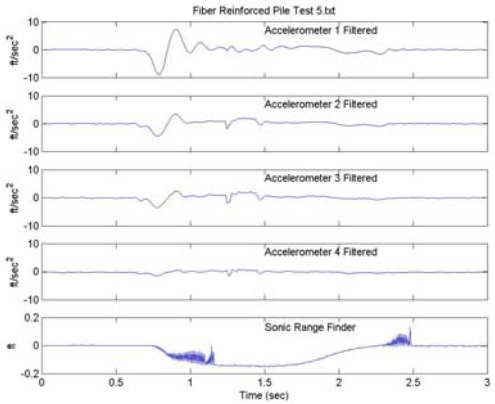
Fiber Reinforced Pile Test 5.txt
Accelerometer 1 Filtered
Accelerometer 2 Filtered
Accelerometer 3 Filtered
Accelerometer 4 Filtered
Sonic Range Finder
ft/sec²
ft
Time (sec)

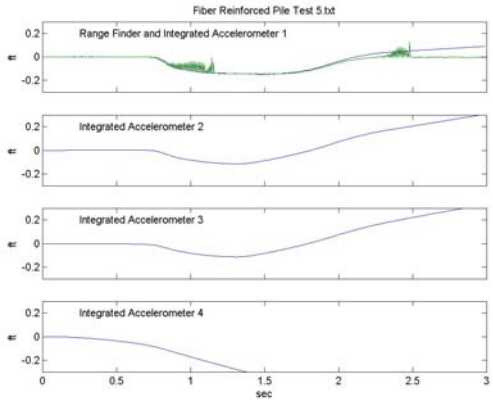
Fiber Reinforced Pile Test 5.txt
Range Finder and Integrated Accelerometer 1
Integrated Accelerometer 2
Integrated Accelerometer 3
Integrated Accelerometer 4
ft
sec

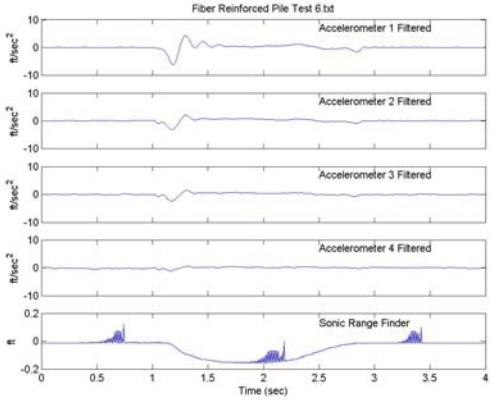
Fiber Reinforced Pile Test 6.txt
Accelerometer 1 Filtered
Accelerometer 2 Filtered
Accelerometer 3 Filtered
Accelerometer 4 Filtered
Sonic Range Finder
ft/sec²
ft
Time (sec)

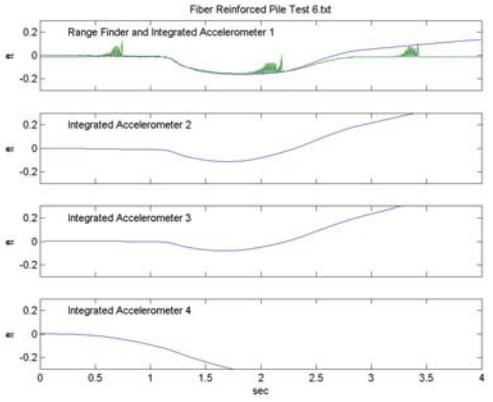
Fiber Reinforced Pile Test 6.txt
Range Finder and Integrated Accelerometer 1
Integrated Accelerometer 2
Integrated Accelerometer 3
Integrated Accelerometer 4
ft
sec

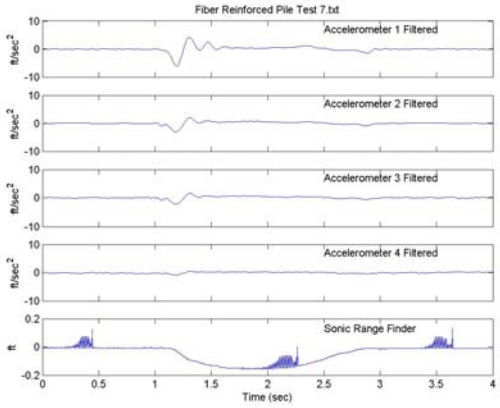
Fiber Reinforced Pile Test 7.txt
Accelerometer 1 Filtered
Accelerometer 2 Filtered
Accelerometer 3 Filtered
Accelerometer 4 Filtered
Sonic Range Finder
ft/sec²
ft
Time (sec)

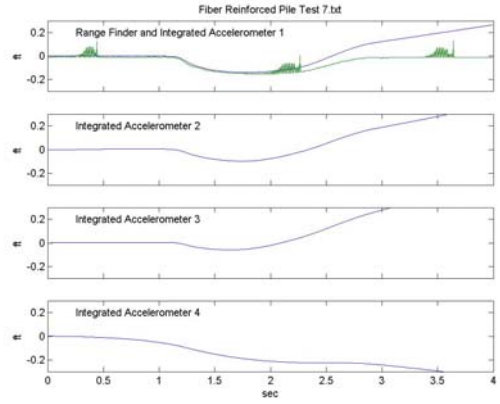
Fiber Reinforced Pile Test 7.txt
Range Finder and Integrated Accelerometer 1
Integrated Accelerometer 2
Integrated Accelerometer 3
Integrated Accelerometer 4
ft
sec

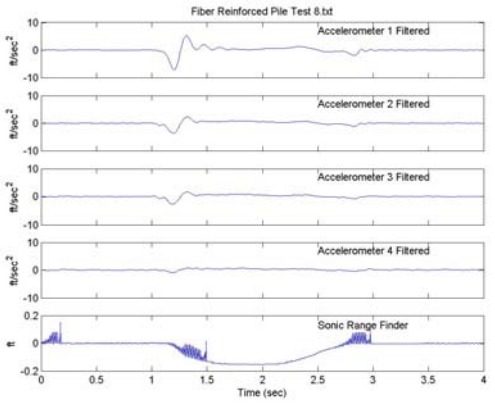
Fiber Reinforced Pile Test 8.txt
Accelerometer 1 Filtered
Accelerometer 2 Filtered
Accelerometer 3 Filtered
Accelerometer 4 Filtered
Sonic Range Finder
ft/sec²
ft
Time (sec)

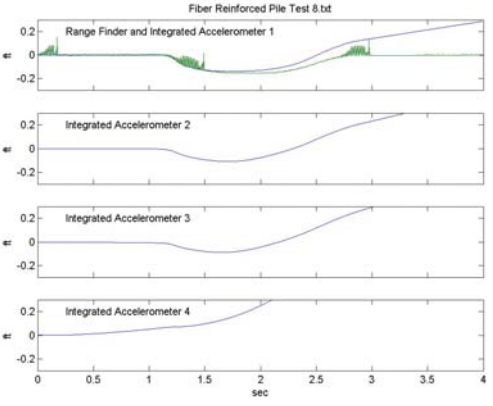
Fiber Reinforced Pile Test 8.txt
Range Finder and Integrated Accelerometer 1
Integrated Accelerometer 2
Integrated Accelerometer 3
Integrated Accelerometer 4
ft
sec

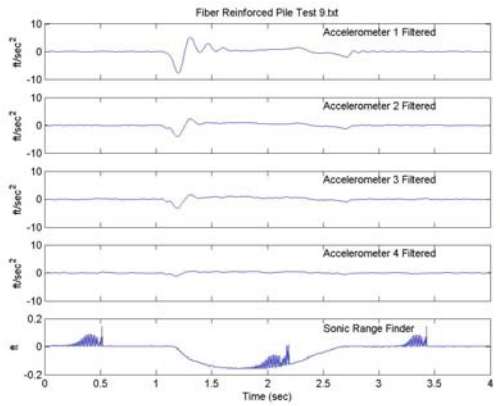
Fiber Reinforced Pile Test 9.txt
Accelerometer 1 Filtered
Accelerometer 2 Filtered
Accelerometer 3 Filtered
Accelerometer 4 Filtered
Sonic Range Finder
ft/sec²
ft
Time (sec)

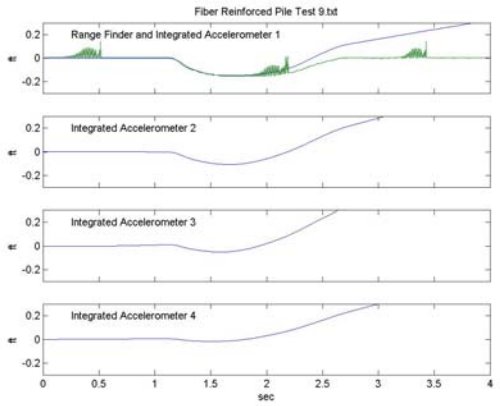
Fiber Reinforced Pile Test 9.txt
Range Finder and Integrated Accelerometer 1
Integrated Accelerometer 2
Integrated Accelerometer 3
Integrated Accelerometer 4
ft
sec

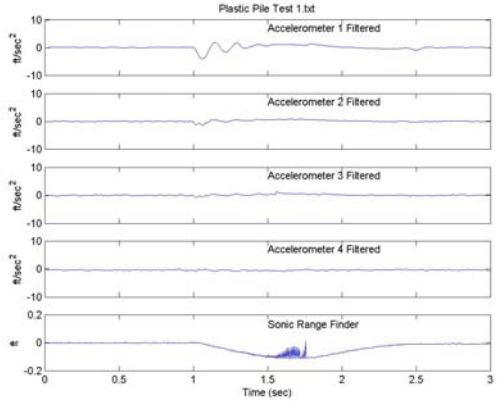
Plastic Pile Test 1.txt
Accelerometer 1 Filtered
Accelerometer 2 Filtered
Accelerometer 3 Filtered
Accelerometer 4 Filtered
Sonic Range Finder
ft/sec²
ft
Time (sec)

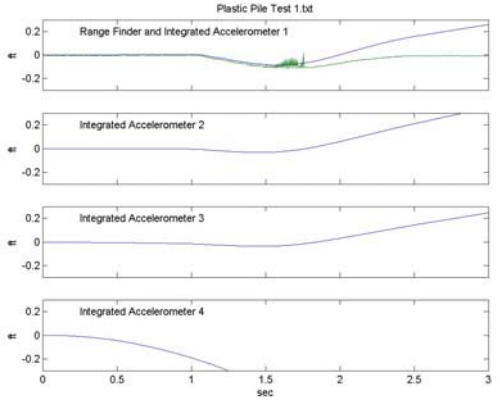
Plastic Pile Test 1.txt
Range Finder and Integrated Accelerometer 1
Integrated Accelerometer 2
Integrated Accelerometer 3
Integrated Accelerometer 4
ft
sec

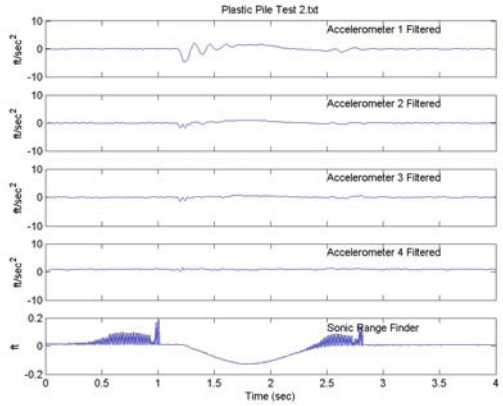
Plastic Pile Test 2.txt
Accelerometer 1 Filtered
Accelerometer 2 Filtered
Accelerometer 3 Filtered
Accelerometer 4 Filtered
Sonic Range Finder
ft/sec²
ft
Time (sec)

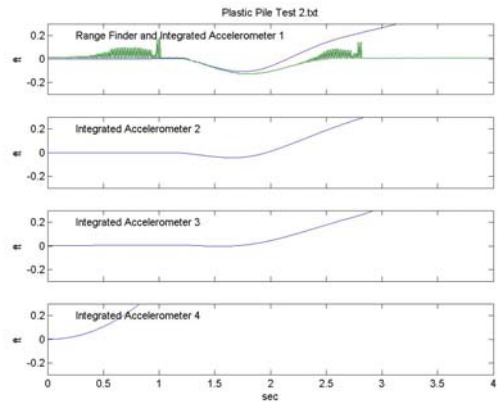
Plastic Pile Test 2.txt
Range Finder and Integrated Accelerometer 1
Integrated Accelerometer 2
Integrated Accelerometer 3
Integrated Accelerometer 4
ft
sec

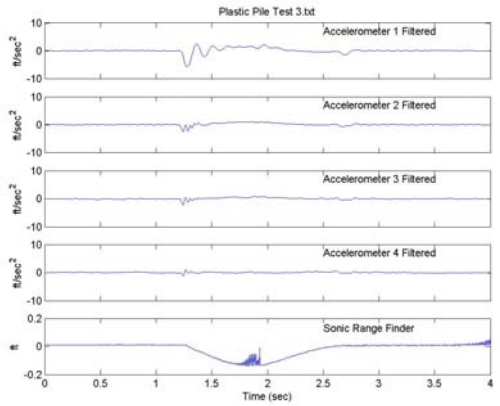
Plastic Pile Test 3.txt
Accelerometer 1 Filtered
Accelerometer 2 Filtered
Accelerometer 3 Filtered
Accelerometer 4 Filtered
Sonic Range Finder
ft/sec²
ft
Time (sec)

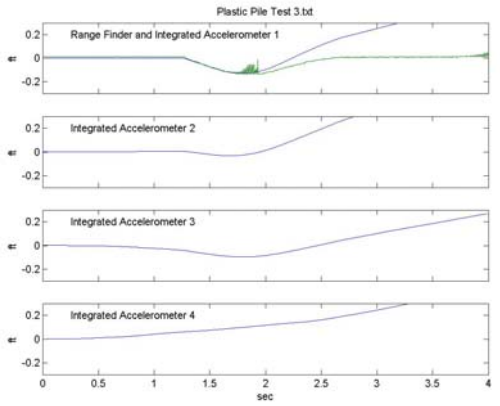
Plastic Pile Test 3.txt
Range Finder and Integrated Accelerometer 1
Integrated Accelerometer 2
Integrated Accelerometer 3
Integrated Accelerometer 4
ft
sec

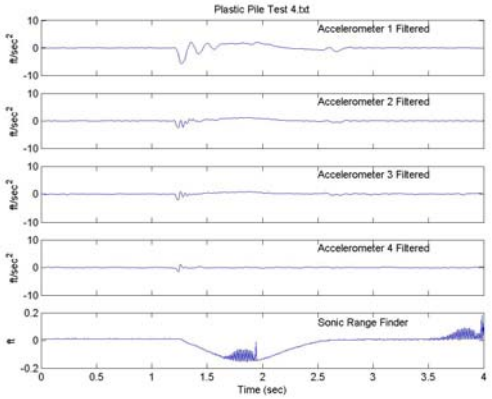
Plastic Pile Test 4.txt
Accelerometer 1 Filtered
Accelerometer 2 Filtered
Accelerometer 3 Filtered
Accelerometer 4 Filtered
Sonic Range Finder
ft/sec²
ft
Time (sec)

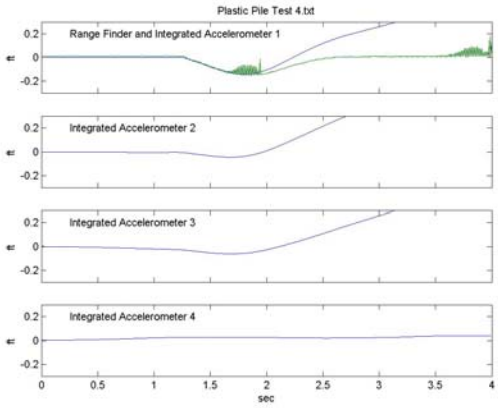
Plastic Pile Test 4.txt
Range Finder and Integrated Accelerometer 1
Integrated Accelerometer 2
Integrated Accelerometer 3
Integrated Accelerometer 4
ft
sec

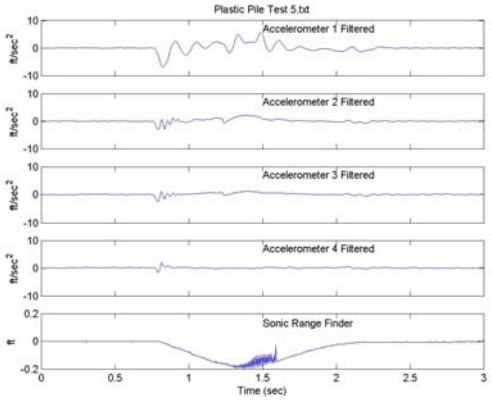
Plastic Pile Test 5.txt
Accelerometer 1 Filtered
Accelerometer 2 Filtered
Accelerometer 3 Filtered
Accelerometer 4 Filtered
Sonic Range Finder
ft/sec²
ft
Time (sec)

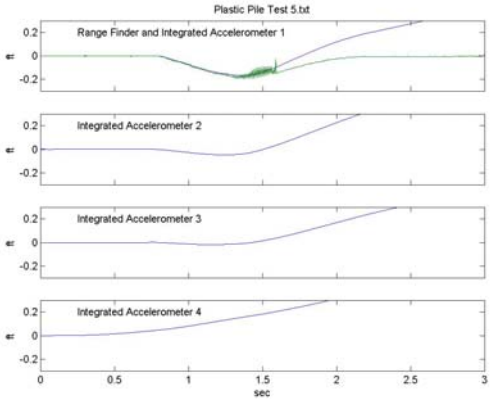
Plastic Pile Test 5.txt
Range Finder and Integrated Accelerometer 1
Integrated Accelerometer 2
Integrated Accelerometer 3
Integrated Accelerometer 4
ft
sec

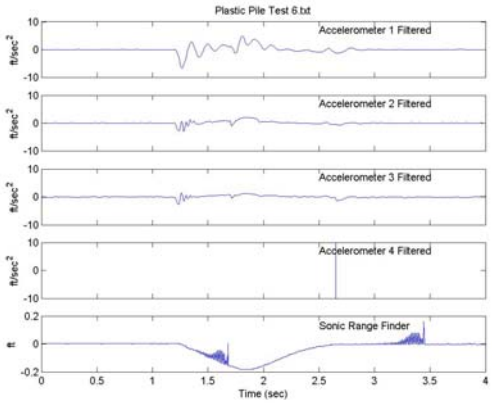
Plastic Pile Test 6.txt
Accelerometer 1 Filtered
Accelerometer 2 Filtered
Accelerometer 3 Filtered
Accelerometer 4 Filtered
Sonic Range Finder
ft/sec²
ft
Time (sec)

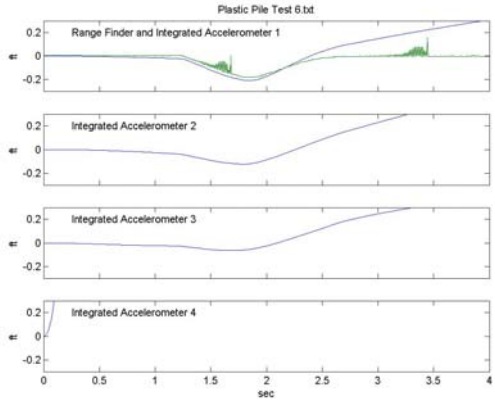
Plastic Pile Test 6.txt
Range Finder and Integrated Accelerometer 1
Integrated Accelerometer 2
Integrated Accelerometer 3
Integrated Accelerometer 4
ft
sec